Research article

JHEP|Reports

A new NRF2 activator for the treatment of human metabolic dysfunction-associated fatty liver disease

Adel Hammoutene,[1,2] Samira Laouirem,[1] Miguel Albuquerque,[1,3] Nathalie Colnot,[3] Angélique Brzustowski,[1] Dominique Valla,[1] Nicolas Provost,[2] Philippe Delerive,[2] Valérie Paradis [1,3,*], on behalf of the QUID-NASH Research Group

[1]*Université Paris Cité, Inserm, Centre de Recherche sur l'inflammation, F-75018 Paris, France;* [2]*Cardiovascular and Metabolic Diseases Research, Institut de Recherches Servier, Suresnes, France;* [3]*Département de Pathologie, Hôpital Beaujon, Assistance Publique-Hôpitaux de Paris, Clichy, France*

JHEP Reports **2023.** https://doi.org/10.1016/j.jhepr.2023.100845

Background & Aims: Oxidative stress triggers metabolic-associated fatty liver disease (MAFLD) and fibrosis. Previous animal studies demonstrated that the transcription factor nuclear factor (erythroid-derived 2)-like 2 (NRF2), the master regulator of antioxidant response, protects against MAFLD and fibrosis. S217879, a next generation NRF2 activator has been recently shown to trigger diet-induced steatohepatitis resolution and to reduce established fibrosis in rodents. Our aim was to evaluate the therapeutic potential of S217879 in human MAFLD and its underlying mechanisms using the relevant experimental 3D model of patient-derived precision cut liver slices (PCLS).

Methods: We treated PCLS from 12 patients with varying stages of MAFLD with S217879 or elafibranor (peroxisome proliferator-activated receptor [PPAR]α/δ agonist used as a referent molecule) for 2 days. Safety and efficacy profiles, steatosis, liver injury, inflammation, and fibrosis were assessed as well as mechanisms involved in MAFLD pathophysiology, namely antioxidant response, autophagy, and endoplasmic reticulum-stress.

Results: Neither elafibranor nor S217879 had toxic effects at the tested concentrations on human PCLS with MAFLD. PPARα/δ and NRF2 target genes (pyruvate dehydrogenase kinase 4 [*PDK4*], fibroblast growth factor 21 [*FGF21*], and NAD(P)H quinone dehydrogenase 1 [*NQO1*], heme oxygenase 1 [*HMOX1*], respectively) were strongly upregulated in PCLS in response to elafibranor and S217879, respectively. Compared with untreated PCLS, elafibranor and S217879-treated slices displayed lower triglycerides and reduced inflammation (*IL-1β*, *IL-6*, chemokine (C–C motif) ligand 2 [*CCL2*]). Additional inflammatory markers (chemokine (C–C motif) ligand 5 [*CCL5*], stimulator of interferon genes [STING], intercellular adhesion molecule-1 [ICAM-1], vascular cell adhesion molecule-1 [VCAM-1]) were downregulated by S217879. S217879 but not elafibranor lowered DNA damage (phospho-Histone H2A.X [p-H2A.X], *RAD51*, X-ray repair cross complementing 1 [*XRCC1*]) and apoptosis (cleaved caspase-3), and inhibited fibrogenesis markers expression (alpha smooth muscle actin [α-SMA], collagen 1 alpha 1 [*COL1A1*], collagen 1 alpha 2 [*COL1A2*]). Such effects were mediated through an improvement of lipid metabolism, activated antioxidant response and enhanced autophagy, without effect on endoplasmic reticulum-stress.

Conclusions: This study highlights the therapeutic potential of a new NRF2 activator for MAFLD using patient-derived PCLS supporting the evaluation of NRF2 activating strategies in clinical trials.

Impact and implications: Oxidative stress is a major driver of metabolic-associated fatty liver disease (MAFLD) development and progression. Nuclear factor (erythroid-derived 2)-like 2, the master regulator of the antioxidative stress response, is an attractive therapeutic target for the treatment of MAFLD. This study demonstrates that S217879, a new potent and selective nuclear factor (erythroid-derived 2)-like 2 activator, displays antisteatotic effects, lowers DNA damage, apoptosis, and inflammation and inhibits fibrogenesis in human PCLS in patients with MAFLD.

Introduction

Metabolic-associated fatty liver disease (MAFLD) is an expanding health problem with an estimated global prevalence of 25%. MAFLD is associated with obesity, insulin resistance, or type 2 diabetes and other metabolic abnormalities collectively termed metabolic syndrome.[1–4] MAFLD encompasses a spectrum of histological lesions ranging from simple steatosis to steatohepatitis which includes, in addition to steatosis, hepatocellular ballooning, and inflammation with varying degrees of fibrosis.[5–7] MAFLD can progress to cirrhosis and hepatocellular carcinoma and is projected to become the leading indication for liver transplantation in the next decades.[8–10] Despite its prevalence and severity, there is still no approved therapy for this condition[11] and this can be attributed, at least in part, to the poor translational value of animal and *in vitro* models used in

Keywords: NRF2; S217879; Elafibranor; MAFLD; NASH; Oxidative stress; PCLS; Inflammation; Fibrosis.

Received 29 December 2022; received in revised form 9 June 2023; accepted 20 June 2023; available online 12 July 2023

* Corresponding author. Address: Service de pathologie, Hôpital Beaujon, 100 boulevard du Général Leclerc, 92100 Clichy, France. Tel: +33-1-40-87-54-63; Fax: +33-1-40-87-00-77.

E-mail address: valerie.paradis@aphp.fr (V. Paradis).

preclinical studies, supporting the critical need for more relevant experimental tools.

Oxidative stress is a key pathogenic event that promotes MAFLD progression from steatosis to steatohepatitis and fibrogenesis. During the course of the disease, lipotoxicity and increased levels of reactive oxygen species (ROS) lead to oxidative cellular and DNA damage and to the activation of apoptotic, inflammatory, and fibrotic pathways.[5,12,13] Patients with MAFLD display increased levels of ROS and lipid peroxidation products, excessive systemic and hepatic oxidative stress, and decreased levels of antioxidant enzymes and compounds such as glutathione (GSH).[13–17] The nuclear factor (erythroid-derived 2)-like 2 (NRF2)/Kelch-like ECH-associated protein 1 (KEAP1) system is the master intracellular regulatory system of the antioxidant response to maintain cellular homeostasis.[18] Under physiological conditions, KEAP1 binds and retains NRF2 in the cytoplasm leading to its ubiquitination and proteosomal degradation.[19,20] Upon exposure to oxidative stress, KEAP1 releases NRF2 allowing its nuclear translocation and the induction of NRF2 target genes involved in oxidative stress-induced responses.[21,22] NRF2 plays critical roles in various liver diseases including MAFLD,[23,24] and its liver expression is downregulated in patients with MAFLD and in murine models.[25–27] *Nrf2* deficient animals are more susceptible to diet-induced steatosis and inflammation.[27,28] In contrast, genetic or pharmacological NRF2 activation attenuates diet-induced steatohepatitis and fibrosis,[16,29,30] raising new hopes for MAFLD treatment through NRF2 pharmacological activators. Although encouraging results have been observed in experimental diet-induced steatohepatitis models, NRF2-based therapies have not been evaluated in a clinical setting to date.[24]

The availability of KEAP1 X-ray structure[31] allowed the discovery of second generation NRF2 activators via the direct disruption of its interaction with KEAP1[32] but with limited oral bioavailability.[33] We recently developed a new potent and selective small molecule disrupting KEAP1–NRF2 interaction, S217879, with good pharmacokinetic properties upon oral administration in rodents, with protective effects on diet-induced steatohepatitis and fibrosis murine models.[34] Here, effects of S217879 were assessed in patients with MAFLD using the relevant human precision cut liver slices (PCLS) model, that maintains the morphological and biological organisation of the liver (cell heterogeneity and distribution, extracellular matrix) and all pathological features of the disease.[35] Effects of S217879 were assessed and compared with those of the well-known peroxisome proliferator-activated receptor (PPAR)α/δ agonist, elafibranor.[36–38]

Materials and methods

Human liver samples

Fresh liver tissues were obtained from 12 patients with MAFLD undergoing liver resection at the digestive surgical department of Beaujon Hospital (Clichy, France) for primary or secondary liver cancer (11/12), or from an explanted liver (1/12). Only liver samples collected within 3 h after surgery were used to minimise ischaemic time and preserve hepatocellular viability. Liver specimens were examined by a pathologist, and samples were taken from the most distal nontumoral tissue. Indications for surgery, MAFLD evaluation and alcohol use are detailed in Table S1. Patients' metabolic features are presented in Table S2. None of the patients had detectable anti-hepatitis C virus antibodies or HBs antigen. All patients gave a written consent to participate the study. This study was approved by the Institutional Review Board CPP SUD MEDITERRANEE V (NCT03634098). The study conformed to the ethical guidelines of the 1975 Declaration of Helsinki.

PCLS generation and treatments

Fresh liver specimens were harvested and immediately kept in cold sterile University of Wisconsin solution (Belzer UW®, Bridge to Life, London, UK). Tissue cores were generated using 8-mm diameter biopsy punches, embedded into 5% low-gelling-temperature agarose (Sigma-Aldrich, Saint Quentin Fallavier, France) and mounted in a tissue slicer (Leica Biosystems VT1200S) filled with Hanks Balanced Salt Solution supplemented with 25 mM D-glucose (Sigma Aldrich, Saint Quentin Fallavier, France), 100 μg/ml streptomycin, 1 μg/ml amphotericin B (Gibco™, Thermo Fisher Scientific, Courtaboeuf, France). Samples of 250 μm thickness PCLS[39] were generated using the following slicing parameters: speed 0.5 mm/s; thickness 250 μm; amplitude 3 mm. PCLS were transferred on 8-μm PET-tissue culture inserts (ThinCert™, Greiner bio-one, Courtaboeuf, France) in six-well plates containing 2 ml William's E Medium (Gibco™, Thermo Fisher Scientific, Courtaboeuf, France) supplemented with 100 IU/ml penicillin and 100 μg/ml streptomycin, 1 μg/ml amphotericin B (Gibco™, Thermo Fisher Scientific, Courtaboeuf, France), and 25 mM D-glucose (Sigma-Aldrich, Saint Quentin Fallavier, France), to maintain the slice in an air–liquid interface and avoid tissue hypoxia.[39–41] After 2 h pre-incubation, medium was replaced with fresh culture medium in the presence or absence of 10 μM elafibranor[42] (Selleckchem S3720, Planegg, Germany) or 3 μM S217879 (synthesised by Servier Medicinal Chemistry department), corresponding to the drug concentration reaching the liver upon oral administration in rodents (30 mg/kg)[34] (dissolved in DMSO, final concentration 0.1%). PCLS were cultivated at 37 °C, 5% CO_2, in normoxic conditions, under continuous orbital agitation (70 rpm) for 48 h. Culture medium was renewed daily. In another set of experiments, PCLS were treated with chloroquine (300 μmol/L, Sigma-Aldrich, Saint Quentin Fallavier, France) for 1 h before the end of the 48-h culture period, to assess autophagic flux. Patients' characteristics for this set of experiments are detailed in Table S3. After 48 h of culture, PCLS were washed in cold phosphate-buffered saline and immediately snap-frozen in liquid nitrogen and stored at -80 °C until processing (for gene, protein, ATP, and triglycerides experiments) or fixed in 10% formalin and embedded in paraffin for histology analyses as described in the Supplementary information.

Statistics

Data are expressed as mean ± SEM. Comparisons were performed using the paired Wilcoxon *t* test. All tests were two-sided and a significance level of 0.05 was used. Statistical analyses and figures were performed/created using GraphPad Prism 9 (GraphPad Software, San Diego, CA, USA) for Windows 11.

Results

Drug safety and efficacy

We first tested liver slices viability in response to 48 h of treatment with elafibranor (10 μM)[42] or S217879 (3 μM) or vehicle (DMSO, 0.1%). No effects of elafibranor or S217879 on PCLS

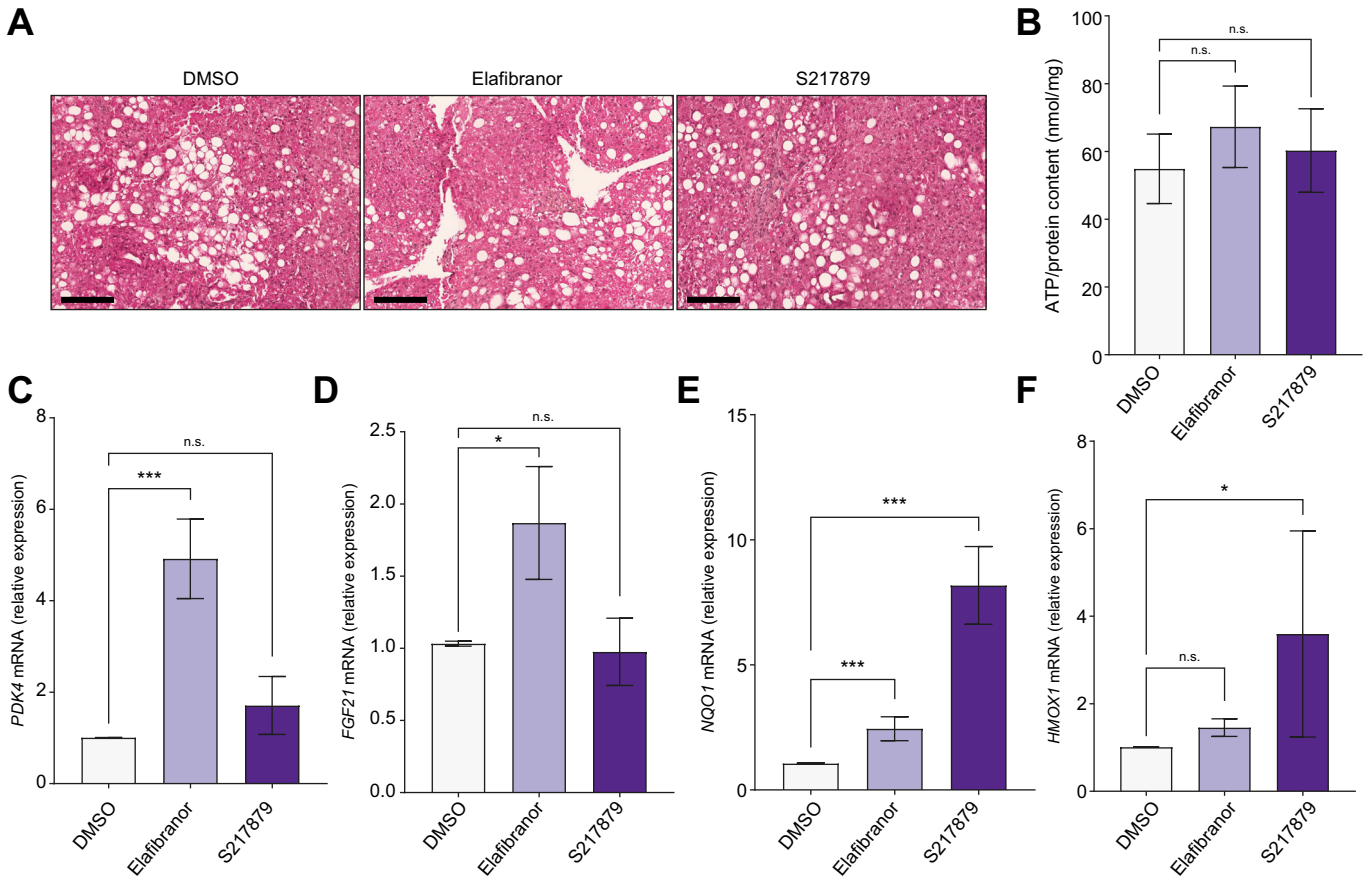

Fig. 1. Drug safety and efficacy. Human PCLS were generated from the liver of patients with MAFLD (n = 12) and treated with elafibranor (10 μM) or S217879 (3 μM) or vehicle (DMSO, 0.1%) for 2 days. (A) Representative images of H&E staining of human PCLS used for histological analysis of slice morphology. Scale bar: 200 μm. (B) Quantification of ATP content in human PCLS (ATP/protein content ratio). (C) qPCR analysis of PPARα/δ target genes expression *PDK4* and (D) *FGF21*. (E) qPCR analysis of NRF2 target genes expression *NQO1* and (F) *HMOX1*. Data are expressed as mean ± SEM. **p* <0.05; ****p* <0.001; ns, not significant (Wilcoxon paired *t* test). *FGF21*, fibroblast growth factor 21; *HMOX1*, heme oxygenase 1, MAFLD, metabolic-associated fatty liver disease; *NQO1*, NAD(P)H quinone dehydrogenase 1; NRF2, nuclear factor (erythroid-derived 2)-like 2; PCLS, precision cut liver slices; *PDK4*, pyruvate dehydrogenase kinase 4; *PPAR*, peroxisome proliferator-activated receptor; qPCR, quantitative PCR.

morphology were observed at histological examination (Fig. 1A). The ATP/protein content ratio, as a reflect of slices viability,[39] was similar between elafibranor or S217879 and DMSO-treated PCLS (Fig. 1B). Of note, neither ATP nor protein contents were modulated by elafibranor or S217879 treatment (Fig. S1A and B). Furthermore, RNA content as well as aspartate aminotransferase (AST) and lactate dehydrogenase (LDH) leakage in culture supernatants were not significantly affected by both treatments (Fig. S1C–E).

We then confirmed target engagement induced by both molecules by assessing the expression of their respective target genes. PPARα/δ target genes pyruvate dehydrogenase kinase 4 (*PDK4*) and fibroblast growth factor 21 (*FGF21*) were upregulated in elafibranor but not in S217879-treated PCLS (Fig. 1C and D). Similarly, NRF2 target genes NAD(P)H quinone dehydrogenase 1 (*NQO1*) and heme oxygenase 1 (*HMOX1*) were strongly induced by S217879 (Fig. 1E and F). Of note, *NQO1* expression, but not *HMOX1* expression, was slightly induced by elafibranor (Fig. 1E and F). Collectively, these data indicate that elafibranor and S217879 have no hepatotoxic effects, and effectively induce their respective target genes in human PCLS with MAFLD at the tested concentrations.

S217879 improves features of steatohepatitis in human PCLS with MAFLD

To assess effects of elafibranor and S217879 on liver metabolic features, we first evaluated glucose-6-phosphatase (*G6PC*) gene expression, a key enzyme of neoglucogenesis. Compared with vehicle-treated PCLS, *G6PC* expression was reduced by S217879 but not by elafibranor (Fig. 2A). In line with this, glucose concentration in culture supernatants was not affected by elafibranor and was reduced after S217879 treatment (Fig. S2A). We then assessed whether these treatments were able to modulate steatosis. No changes in steatosis using semiquantitative score could be evidenced at histological examination between elafibranor or S217879 and DMSO-treated PCLS (Fig. 1A). For a more precise analysis of steatosis, we measured triglycerides content in PCLS and observed that triglycerides on protein content ratio was significantly lower in both elafibranor and S217879-treated PCLS compared with the vehicle (Fig. 2B). We then sought to identify which metabolic pathways were involved in this improvement of triglycerides content by assessing gene expression of key players of lipid metabolism. Elafibranor significantly increased peroxisomal acyl-coenzyme A oxidase-1 (*ACOX1*) and carnitine palmitoyltransferase-1-alpha (*CPT1A*) gene expression

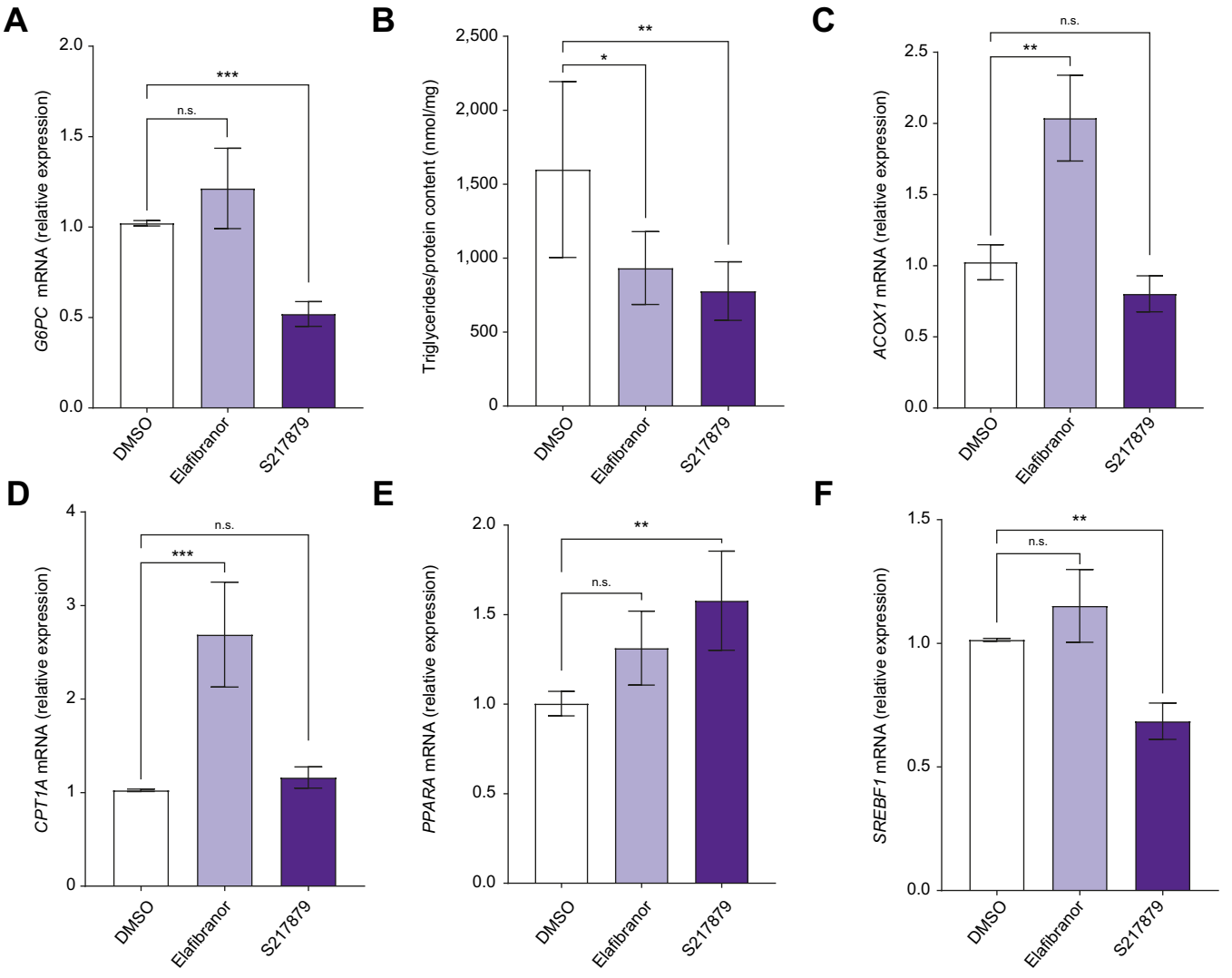

Fig. 2. Effects of elafibranor and S217879 treatments on liver metabolic features. Human PCLS were generated from the liver of patients with MAFLD (n = 12) and treated with elafibranor (10 μM) or S217879 (3 μM) or vehicle (DMSO, 0.1%) for 2 days. (A) qPCR analysis of *G6PC* expression in human PCLS. (B) Quantification of triglycerides content in human PCLS (triglycerides/protein content ratio). (C) qPCR analysis of *ACOX1*, (D) *CPT1A*, (E) *PPARA* and (F) *SREBF1* expression in human PCLS. Data are expressed as mean ± SEM. $^{*}p$ <0.05; $^{**}p$ <0.01; $^{***}p$ <0.001; ns, not significant (Wilcoxon paired *t* test). *ACOX1*, peroxisomal acyl-coenzyme A oxidase 1; *CPT1A*, carnitine palmitoyl transferase 1 alpha; G6PC, glucose-6-phosphatase; MAFLD, metabolic-associated fatty liver disease; PCLS, precision cut liver slices; *PPARA*, peroxisome proliferator-activated receptor-alpha; qPCR, quantitative PCR; *SREBF1*, sterol regulatory element-binding protein-1.

(Fig. 2C and D), both enzymes involved in fatty acids beta-oxidation. However, S217879 significantly increased peroxisome proliferator-activated receptor-alpha (*PPARA*) gene expression, also involved in fatty acid beta-oxidation, and significantly downregulated sterol regulatory element-binding protein-1 (*SREBF1*) and fatty acid synthase (*FASN*) (Fig. 2E and F, Fig. S2B) gene expression, both involved in *de novo* lipogenesis. Elafibranor had no effect on *PPARA*, *SREBF1*, and *FASN* expression (Fig. 2E and F, Fig. S2B), and S217879 had no effect on *ACOX1* and *CPT1A* (Fig. 2C and D) expression. These results indicate that both elafibranor and S217879 improve steatosis, whereas only S217879 improves glucose metabolism in human PCLS with MAFLD.

Oxidative stress promotes liver injury and DNA damage that initiate hepatic cell death in MAFLD.[43–45] We tested whether elafibranor and S217879 were able to lower liver injury in human PCLS with MAFLD. As mentioned above, AST and LDH levels in culture supernatants were not modulated neither by elafibranor nor by S217879 treatments (Fig. S1D and E). As oxidative stress initiates apoptosis by inducing DNA damage,[44] we next investigated the expression of several markers of this pathway. Immunohistochemical and immunoblot analysis of phospho-Histone H2A.X (p-H2A.X) displayed less double-strand DNA damage in S217879-treated PCLS but not in elafibranor-treated slices (Fig. 3A and B). Consequently, liver expression of *RAD51* (double-strand DNA damage repair enzyme), and X-ray repair cross complementing 1 (*XRCC1*; single-strand DNA damage repair enzyme), was significantly and specifically reduced in S217879-treated PCLS (Fig. 3C and D). Accordingly, immunohistochemical analysis of cleaved caspase-3 on PCLS sections revealed that only S217879 lowered cleaved caspase-3 area when compared with untreated slices (Fig. 3E). These

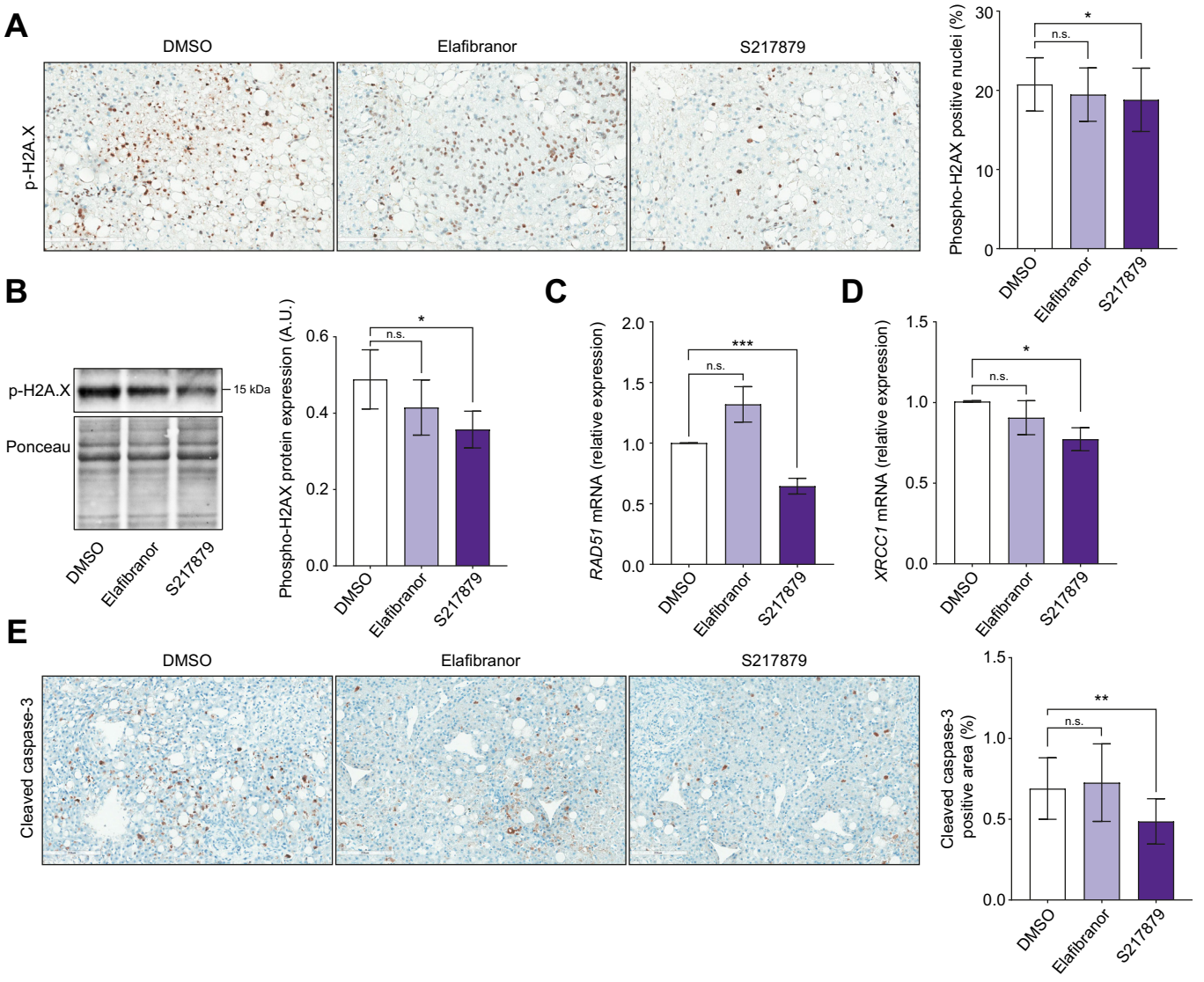

Fig. 3. S217879 but not elafibranor reduces liver DNA damage and apoptosis. Human PCLS were generated from the liver of patients with MAFLD (n = 12) and treated with elafibranor (10 μM) or S217879 (3 μM) or vehicle (DMSO, 0.1%) for 2 days. (A) Immunohistochemical analysis of p-H2A.X-positive nuclei (%) on human PCLS sections. Scale bar: 200 μm. (B) Immunoblot analysis of liver p-H2A.X expression in human PCLS. (C) qPCR analysis of *RAD51* and (D) *XRCC1* expression in human PCLS. (E) Immunohistochemical analysis of cleaved Caspase-3 positive area (%) on human PCLS sections. Scale bar: 200 μm. Data are expressed as mean ± SEM. *p <0.05; **p <0.01; ***p <0.001; ns, not significant (Wilcoxon paired t test). MAFLD, metabolic-associated fatty liver disease; PCLS, precision cut liver slices; p-H2A.X, phospho-Histone H2A.X; qPCR, quantitative PCR; XRCC1, X-ray repair cross complementing 1.

results demonstrate that S217879, rather than elafibranor, reduces liver apoptosis by, at least in part, improving hepatic DNA damage.

Having observed that S217879 reduces steatosis, liver DNA damage, and apoptosis, we hypothesised that this new NRF2 activator could also display anti-inflammatory properties in human PCLS with MAFLD. We first confirmed that elafibranor improved liver inflammation. As expected,[36,37] elafibranor significantly reduced *IL-1β*, *IL-6* (Fig. 4A and B) and chemokine (C–C motif) ligand 2 (*CCL2*) (Fig. S3A) liver gene expression. However, elafibranor had no effect on chemokine (C–C motif) ligand 5 (*CCL5*) gene expression (Fig. S3B), vascular cell adhesion molecule-1 (VCAM-1) and intercellular adhesion molecule-1 (ICAM-1) protein expression (Fig. 4C and D), both markers of vascular inflammation, stimulator of interferon genes (STING) protein expression (Fig. S3C), a key player of the cyclic GMP–AMP synthase (cGAS)–stimulator of interferon genes (STING) signalling pathway involved in innate immune response in MAFLD,[46,47] and did not change macrophages markers expression as assessed on CD68 immunohistochemical analysis (Fig. 4E). Compared with vehicle-treated PCLS, S21879-treated slices had a significant lower gene expression of *IL-1β*, *IL-6* (Fig. 4A and B), *CCL2* and *CCL5* (Fig. S3A and B). VCAM-1, ICAM-1 (Fig. 4C and D) and STING (Fig. S3C) protein expression was significantly reduced in S217879-treated PCLS compared with the vehicle. Moreover, the CD68-positive area was reduced in S217879-treated PCLS compared with untreated slices (Fig. 4E). Interestingly, similar effects of elafibranor and S217879 treatments were observed in PCLS from patients with advanced liver fibrosis (F3–4, n = 9) (Fig. S4A–H). These results indicate that both elafibranor and

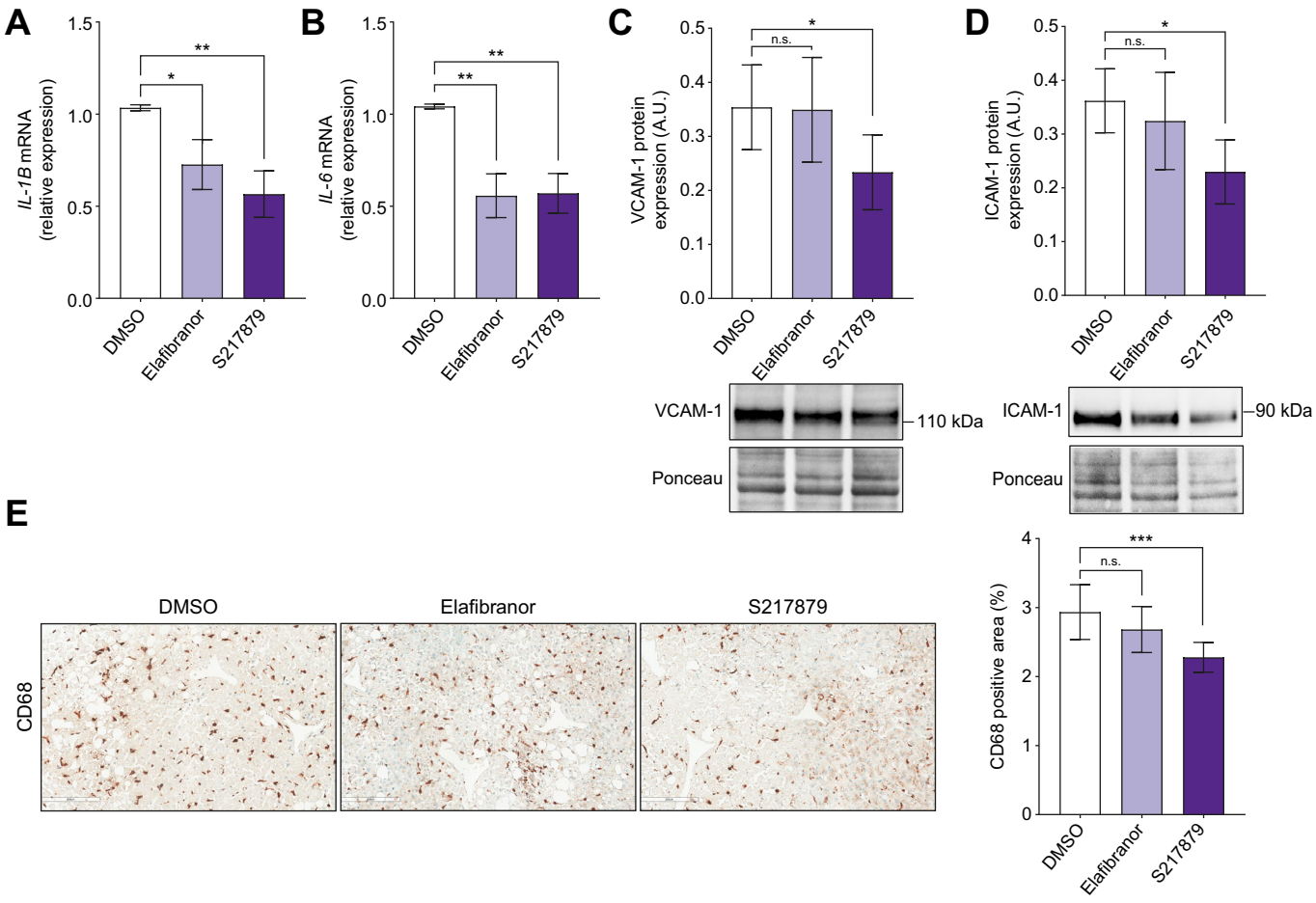

Fig. 4. Elafibranor and S217879 reduce liver inflammation. Human PCLS were generated from the liver of patients with MAFLD (n = 12) and treated with elafibranor (10 μM) or S217879 (3 μM) or vehicle (DMSO, 0.1%) for 2 days. (A) qPCR analysis of *IL-1β* and (B) *IL-6* expression in human PCLS. (C) Immunoblot analysis of VCAM-1 and (D) ICAM-1 expression in human PCLS. (E) Immunohistochemical analysis of CD68 positive area (%) in human PCLS. Scale bar: 200 μm. Data are expressed as mean ± SEM. **p* <0.05; ***p* <0.01; ****p* <0.001; ns, not significant (Wilcoxon paired *t* test). ICAM-1, intercellular adhesion molecule-1; MAFLD, metabolic-associated fatty liver disease; PCLS, precision cut liver slices; qPCR, quantitative PCR; VCAM-1, vascular cell adhesion molecule-1.

S217879 inhibit liver inflammatory pathways in human PCLS with MAFLD with the strongest anti-inflammatory response induced by S217879.

Collectively, these observations demonstrate that S217879 displays therapeutic properties against MAFLD in human liver samples.

S217879 reduces fibrosis markers expression in human PCLS with MAFLD

Sustained liver cell death and inflammation trigger hepatic stellate cells activation and fibrogenesis in MAFLD,[5] so that prompted us to evaluate effects of both drugs on fibrogenesis. As expected,[37] elafibranor had no effect on liver fibrogenesis markers expression in human PCLS with MAFLD (*ACTA2*, alpha smooth muscle actin [α-SMA], collagen 1 alpha 1 [*COL1A1*], and collagen 1 alpha 2 [*COL1A2*]) (Fig. 5). By contrast, qPCR, immunohistochemistry, and immunoblot analyses showed a reduction of α-SMA expression, a marker of hepatic stellate cells activation (Fig. 5A–C) in S217879-treated PCLS. Accordingly, this reduced hepatic stellate cell activation was associated with a decrease in *COL1A1* and *COL1A2* expression (Fig. 5D and E). Importantly, S217879 treatment was also effective to inhibit fibrogenesis markers expression specifically in PCLS from patients with advanced fibrosis (F3–4, n = 9) (Fig. S4I and J). Of note, fibrosis deposition evaluated on Sirius Red staining using quantitative approaches remained unchanged between elafibranor or S217879 and untreated PCLS, likely because of the short duration of treatment (Fig. S5).

S217879 activates the antioxidant response and autophagy but does not modulate ER-stress in human PCLS with MAFLD

To dissect cellular mechanisms by which elafibranor and S217879 improve MAFLD features, we first evaluated the antioxidant response induced by both treatments. As expected,[38,48] elafibranor treatment tended to increase total GSH content (Fig. 6A), glutathione S-transferase alpha-2 (*GSTA2*) and glutathione peroxidase 2 (*GPX2*) gene expression without reaching statistical significance, but significantly induced glutathione peroxidase-3 (*GPX3*) gene expression (Fig. 6B–D), all detoxifying enzymes involved in antioxidant response. At the protein level, elafibranor had no significant effect on detoxifying enzymes GPX2, glutathione S-transferase mu-2 (GSTM2), microsomal glutathione S-transferase-1 (MGST1), glutathione S-transferase theta-1 (GSTT1), and superoxide dismutase (SOD) expression

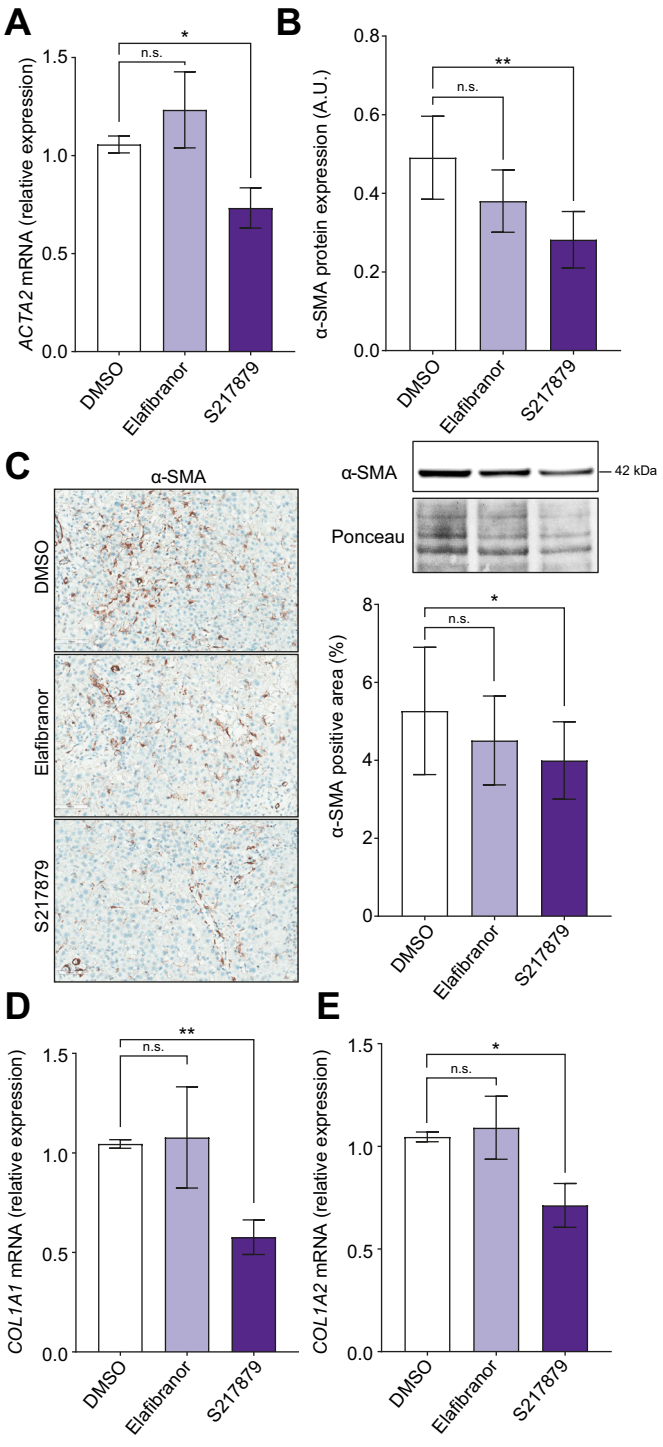

Fig. 5. S217879 but not elafibranor inhibits fibrogenesis. Human PCLS were generated from the liver of patients with MAFLD (n = 12) and treated with elafibranor (10 μM) or S217879 (3 μM) or vehicle (DMSO, 0.1%) for 2 days. (A) qPCR analysis of *ACTA2* expression in human PCLS. (B) Immunoblot analysis of α-SMA expression in human PCLS. (C) Immunohistochemical analysis of α-SMA-positive area (%) on human PCLS sections. Scale bar: 200 μm. (D) qPCR analysis of *COL1A1* and (E) *COL1A2* expression in human PCLS. Data are expressed as mean ± SEM. $^{*}p$ <0.05; $^{**}p$ <0.01; ns, not significant (Wilcoxon paired *t* test). α-SMA, alpha-smooth muscle actin; COL1A, collagen 1-alpha; MAFLD, metabolic-associated fatty liver disease; PCLS, precision cut liver slices; qPCR, quantitative PCR.

(Fig. 6E–H; Fig. S6A–C). Compared with untreated PCLS, S217879-treated slices had a higher GSH content (Fig. 6A) and a strong overexpression of *GSTA2*, *GPX2*, and *GPX3* (Fig. 6B–D). S217879 also significantly increased GPX2, GSTM2, and MGST1 protein expression and had no significant effect on GSTT1 and SOD protein expression (Fig. 6E–H; Fig. S6A–C). As expected, S217879 induced a more pronounced antioxidant response than elafibranor.

Reduced autophagy and increased ER-stress are two early events occurring in MAFLD promoting disease progression.[5,49–51] We hypothesised that beneficial effects of elafibranor and S217879 could be mediated, in addition to their well-known mechanisms of action, through autophagy activation and ER-stress improvement. Microtubule-associated protein light chain-3 (LC3, marker of autophagy) gene (*MAP1LC3B*) and protein (LC3-II) expression were both induced by elafibranor but not by S217879 under basal conditions (Fig. S6D-E). Because LC3 is post-translationally modified (lipidation of LC3-I to form LC3-II), and considering that a lack of effect or a change in LC3-II protein expression can reflect both unmodified or reduced or enhanced autophagic flux,[52] we performed the same experiment by blocking late steps of autophagic flux with chloroquine. As shown in Fig. 6I, LC3-II protein expression was higher in PCLS treated with elafibranor and with S217879 compared with untreated PCLS, suggesting that both treatments activated autophagic flux. We also evaluated C/EBP homologous protein (CHOP) expression which plays an important role in ER-stress-mediated apoptosis and inflammation in MAFLD.[51] Immunoblot analysis revealed that CHOP expression was not modulated by elafibranor or by S217879 (Fig. S6F), suggesting that both treatments do not act directly on ER-stress in human PCLS with MAFLD. Collectively, our results indicate that elafibranor and S217879 may work, in addition to their well-known mechanisms of action, via autophagy activation in the liver.

To broaden in the analysis of the mechanisms by which elafibranor and S217879 elicit their properties in human PCLS with MAFLD, we performed an RNA-sequencing analysis on liver total RNA. A total of 150 and 344 genes were significantly differentially expressed between elafibranor (76 up/74 down) and S217879 (100 up/244 down) *vs.* vehicle-treated PCLS (adjusted *p* value cut-off <0.05), respectively (Fig. 7A, Table S6). These transcriptional changes were further explored by gene set-enrichment analysis, which first confirmed the potent induction of the antioxidant response by S217879. Indeed, the ROS pathway was the most affected pathway in S217879-treated PCLS with a strong enrichment in antioxidant genes (Fig. 7B–C, Figs. S7A, S8, Table S6). As expected, elafibranor had a less pronounced effect on antioxidant pathways (Fig. 7B and C, Figs. S7A and S8, Table S6). Gene set-enrichment analysis also confirmed the protective properties of both treatments against steatohepatitis since inflammatory pathways such as 'inflammatory response' and 'tumour necrosis factor alpha (TNFA) signalling' were ranked among the most downregulated pathways upon elafibranor and S217879 treatments, with a more pronounced effect observed in S217879-treated PCLS (Fig. 7B and D, Fig. S8, Table S6). S217879 treatment additionally and specifically inhibited the apoptosis pathway, whereas elafibranor had no significant effect on this pathway (Figs. S7B and S8, Table S6). More interestingly, pathways and genes involved in fibrosis such as 'extracellular matrix structural constituent' were significantly downregulated by S217879, but not by

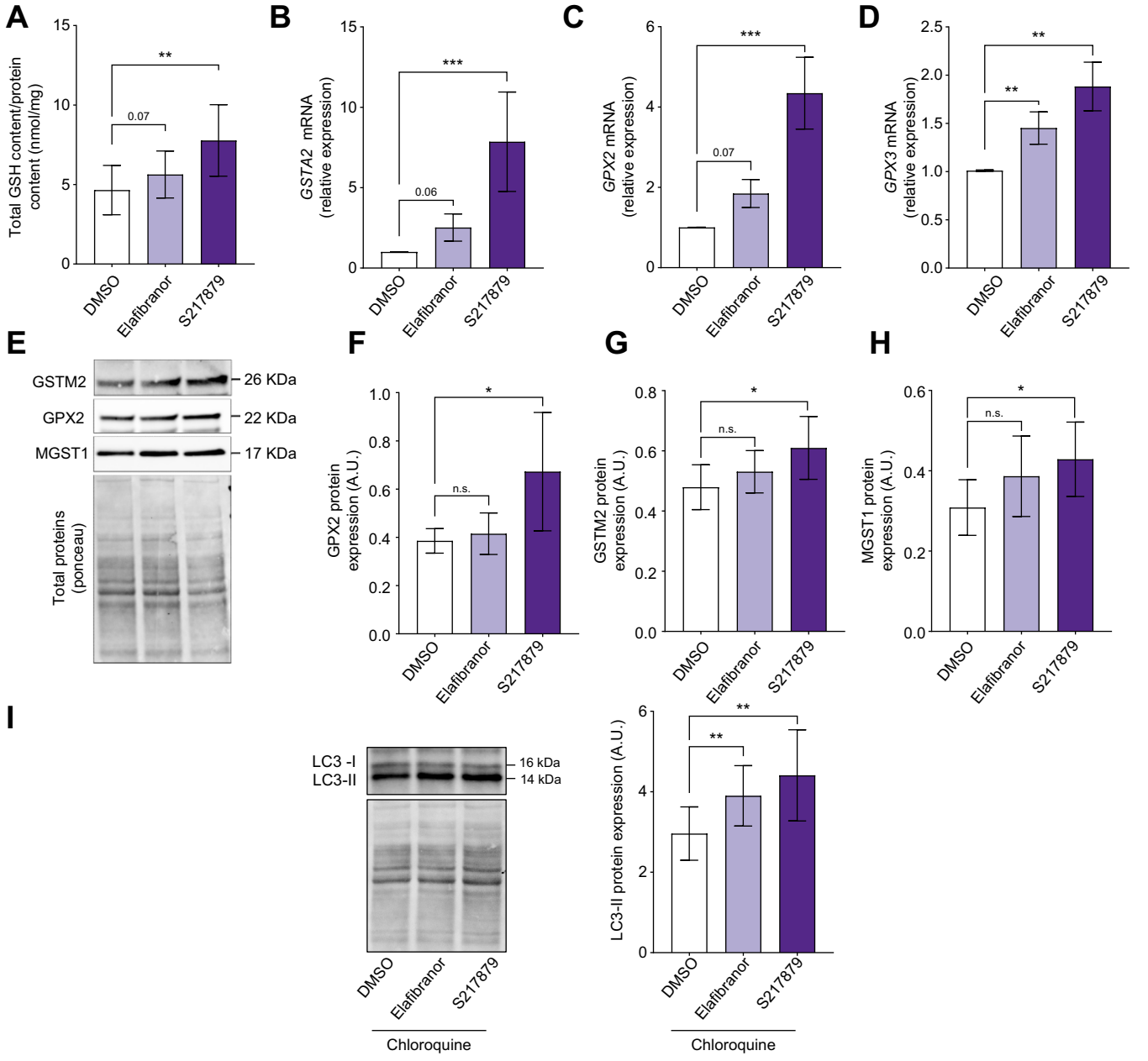

Fig. 6. Elafibranor and S217879 induce antioxidative stress response and enhance autophagy. Human PCLS were generated from the liver of patients with MAFLD (n = 12) and treated with elafibranor (10 μM) or S217879 (3 μM) or vehicle (DMSO, 0.1%) for 2 days. (A) Quantification of total GSH content in human PCLS (GSH/protein content ratio). (B) qPCR analysis of *GSTA2*, (C) GPX2 and (D) *GPX3* expression in human PCLS. (E) Representative western blotting of GSTM2, GPX2 and MGST1 expression. (F) Quantification of GPX2, (G) GSTM2, and (H) MGST1 protein expression. (I) Immunoblot analysis of LC3-II expression in human PCLS (n = 11). Chloroquine (300 μM) was added for the last hour of the culture period. Data are expressed as mean ± SEM. $^{*}p$ <0.05; $^{**}p$ <0.01; $^{***}p$ <0.001; ns, not significant (Wilcoxon paired *t* test). GPX2, glutathione peroxidase 2; GPX3, glutathione peroxidase 3; GSH, glutatione; *GSTA2*, glutathione S-transferase alpha-2; GSTM2, glutathione S-transferase Mu 2; LC3, light chain-3; MAFLD, metabolic-associated fatty liver disease; MGST1, microsomal glutathione S-transferase 1; PCLS, precision cut liver slices; qPCR, quantitative PCR.

elafibranor (Fig. 7 and Fig. S8, Table S6), thus confirming our previous observations (Fig. 5). The RNA-sequencing analysis also showed that S217879 but not elafibranor inhibited angiogenesis, that is, a key early event favouring MAFLD progression[53] (Fig. S7C). Finally, the RNA sequencing analysis also confirmed the global more pronounced and additional effects of S217879 compared with those of elafibranor (Figs. S7 and S8, Table S6). A total of 368 genes were significantly differentially expressed between S217879 and elafibranor-treated slices (130 up/238 down; adjusted *p* value cut-off <0.05) (Fig. S9A, Table S6). As expected, antioxidant response was the most upregulated pathway in S217879-treated PCLS compared with elafibranor-treated slices (Fig. S9B–D). Pathways involved in MAFLD pathophysiology related to lipid metabolism

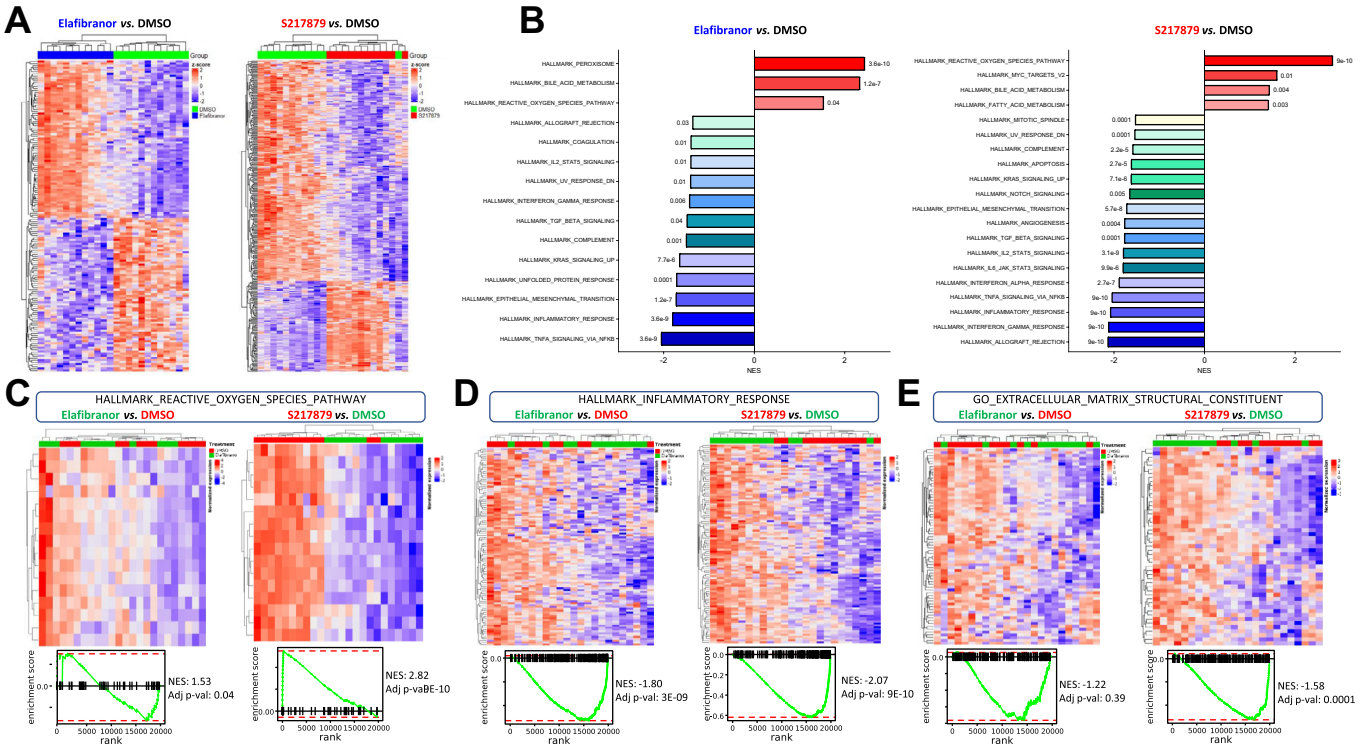

Fig. 7. S217879 treatment induces a potent antioxidant response and inhibits a wide spectrum of pathways involved in MAFLD progression. Human PCLS were generated from the liver of patients with MAFLD (n = 12) and treated with elafibranor (10 μM) or S217879 (3 μM) or vehicle (DMSO, 0.1%) for 2 days. (A) Heatmap of significantly differentially expressed genes from elafibranor and S217879-treated PCLS with MAFLD *vs.* vehicle-treated PCLS (adjusted *p* value cut-off <0.05). (B) Gene set-enrichment analysis of most differentially modulated pathways in elafibranor and S217879-treated PCLS with MAFLD *vs.* vehicle-treated PCLS. (C) Heatmaps and enrichment plots of differentially expressed genes in reactive oxygen species, (D) inflammatory response, and (E) extracellular matrix structural constituent pathways in elafibranor and S217879-treated PCLS *vs.* vehicle treated-PCLS. MAFLD, metabolic-associated fatty liver disease; NES, normalised enrichment score; PCLS, precision cut liver slices.

('adipogenesis'), apoptosis, inflammation ('inflammatory response', 'TNFA signalling', 'IL6 signalling', 'interferon gamma response') and fibrosis ('extracellular matrix structural constituent', 'transforming growth factor-β signalling') were significantly lowered in S217879-treated PCLS when compared with elafibranor-treated slices (Fig. S9B,E–G).

Discussion

This study, based on human PCLS, a relevant *ex vivo* model of MAFLD, provides strong evidence for the therapeutic potential of a new NRF2 activator (S217879) by preventing steatosis, DNA damage, and apoptosis, and inhibiting inflammatory and fibrotic pathways. Such effects were mediated through the improvement of lipid metabolism, a potent induction of antioxidant response and enhanced autophagic flux. Our study extends the first description of S217879, a potent and selective small molecule disrupting KEAP1–NRF2 interaction with good safety and pharmacokinetic properties upon oral administration in two dietary-induced steatohepatitis murine models, that broadly affects key drivers of the disease.[34]

The strength of our study first comes from the use of the *ex vivo* PCLS model from patients with MAFLD to evaluate the early hepatic response to drug candidates. This model of ultra-thin liver slices culture constitutes to date the only tridimensional model that respects at the best the complex organisation of the liver, regarding its cellular heterogeneity and distribution, its micro-environment, and the pathological features of the human disease,[54] overcoming the poor relevance of animal and *in vitro* models, especially in MAFLD. This allowed us the longitudinal study of human liver specimens obtained directly from patients with varying stages of MAFLD (from steatosis to steatohepatitis with and without fibrosis/cirrhosis). In addition, although sex differences are well-known in MAFLD,[55] we included in this study both male and female patients, implying that the observed effects are not restricted to one sex. It should be also emphasised that we included in this study patients with and without type 2 diabetes and observed similar trends in drug responses whatever their diabetes status (*data not shown*), implying that S217879 also effectively works in patients with type 2 diabetes, a favouring condition for steatohepatitis and advanced fibrosis.[6,56] A second strength of the study comes from the use of elafibranor as a reference molecule, which has shown beneficial effects in MAFLD,[36,37] allowing us to validate the efficiency and the translational value of PCLS on the one hand, and to compare effects of S217879 in light of those of elafibranor on the other hand. Interestingly, S217879 exhibited more pronounced protective effects than elafibranor in this model.

The first major finding was the observation that S217879 treatment improved features of MAFLD in human livers through NRF2 pathway activation. First, S217879 lowered glucose concentration in culture supernatants by inhibiting neoglucogenesis,

suggesting that this new molecule could have a potential for diabetes management in patients with MAFLD. Second, we confirmed the antisteatotic effect of elafibranor[36,57] and observed the same effect of S217879 on liver triglycerides content. This antisteatotic effect was mediated by an activation of pathways involved in lipid catabolism, and S217879 additionally inhibited *de novo* lipogenesis pathways. This is in line with previous studies in mice showing that pharmacological and genetic NRF2 activation represses the expression of key factors of fatty acid synthesis with concomitant reduction of hepatic lipids levels.[34,58,59] Besides lipid metabolism, S217879 and elafibranor enhanced autophagy in human PCLS (a prototypic catabolic process). We can yet speculate that the reduction of lipid content could be also attributed to the specific lipid degradation process by autophagy also known as lipophagy. By contrast, Mohs *et al.*[16] reported that hepatic genetic activation of NRF2 by KEAP1 deletion in hepatocytes in mice[60] did not modulate the expression of autophagy related genes. However, the authors analysed autophagy only at the gene expression level whereas autophagy proteins are highly post-translationally modified to modulate autophagic flux.[52,61] Second, we demonstrated that S217879 treatment was able to reduce liver injury and inflammation. Levels of secreted common markers of liver injury (AST, LDH) were not modulated in culture supernatants in this model, whereas we observed a reduction of liver DNA damage that was associated with less apoptosis in S217879 treated slices. This result is in line with the recent description of the protective role of genetic NRF2 activation against oxidative stress-induced DNA damage and consequent apoptosis observed in the hepatocytes-NF-κB essential modulator (NEMO)-deficient genetic steatohepatitis model.[16] A direct link can be made between oxidative stress, DNA damage, and apoptosis when considering that oxidative DNA damage occurs in MAFLD.[43,62,63] and that apoptosis is induced by DNA damage[44,45,64,65] Interestingly, implication of the cGAS-STING pathway in MAFLD recently emerged as a DNA damage sensing pathway recognising DNA leakage in the cytosol that initiates hepatic innate immune response through type-I interferon production.[46,47,63] Our description of a decreased expression of STING in S217879-treated PCLS supports the observation of reduced DNA damage following pharmacological NRF2 activation by S217879. In addition, liver inflammation was also ameliorated in S217879-treated PCLS. This extends previous observations of anti-inflammatory effects of NRF2 activation in rodents[28,29,34,66] but contrasts with recent results described by Mohs *et al.*[16] in which immune cells infiltration and *Il-1β* expression were increased in the liver of hepatocyte-KEAP1-deficient mice in an MAFLD setting. This can be explained by the characteristics of the hepatocyte-NEMO deficient mice model steatohepatitis which displays a constitutive inactivation of the canonical nuclear factor kappa-light-chain-enhancer of activated B cells (NFκB) pathway that regulates inflammation,[60] and the crosstalk between the KEAP1–NRF2 axis and the NFκB pathway, that coordinately regulate cellular responses to resolve inflammation.[67] Interestingly, we also observed a reduction of endothelial inflammation markers (ICAM-1, VCAM-1) in PCLS following NRF2 activator treatment, suggesting that S217879 may also improve liver sinusoidal endothelial cells homeostasis, which is of great importance in the pathophysiology of MAFLD because endothelial inflammation occurs in early steps of the disease and promotes its progression towards advanced steatohepatitis.[50,53] The specific role of NRF2 activation in liver sinusoidal endothelial cells and other liver cell types deserves further studies.

The second major finding of this study was the observation that S217879 lowers fibrogenesis markers expression (Fig. 5), supporting the recent observations made in the amylin liver non-alcoholic steatohepatitis (AMLN) diet-induced steatohepatitis model,[34] and suggesting an antifibrogenic potential of this treatment in humans, even with advanced stages of fibrosis. Importantly, we did not observe antifibrogenic effects of elafibranor, whereas this treatment has raised beneficial effects on liver fibrosis in mice,[57] but failed to improve fibrosis in humans in a clinical trial.[37] These observations obtained in our human PCLS model with MAFLD highlight the limited relevance of murine models and could be explained by the hyper-responsiveness of rodents to PPARα/δ agonism as illustrated by weight loss after elafibranor treatment in mice but not in humans.[37,68] Meanwhile, protective effects of NRF2 activating strategies against liver fibrosis have been described in murine dietary-induced steatohepatitis models by suppressing TGF-β1 signalling and maintaining hepatic stellate cells quiescence.[16,30,34,69,70] In this study, we report for the first time to our knowledge an antifibrotic effect of a pharmacological NRF2 activator in human livers with MAFLD.

All these therapeutic effects against MAFLD and fibrosis were first mediated, as expected, by the promotion of a potent antioxidant response as illustrated by the restoration of the GSH pool in PCLS from patients with MAFLD, and the induction of detoxifying enzymes.[16,34] Of note, PPARα/δ agonism also activated antioxidant response in our model as in others,[38,42,48] but effects of S217879 were obviously stronger than those of elafibranor. Autophagy was also enhanced upon S217879 treatment in human PCLS suggesting that S217879 could improve liver health by rescuing the defect of autophagy that occurs and promotes MAFLD progression.[49,50]

In conclusion, our observations provide for the first time new insights on the therapeutic potential of a new NRF2 activator in a human setting of MAFLD and support the use of NRF2 activating strategies in clinical trials.

Abbreviations

α-SMA, alpha smooth muscle actin; ACOX1, peroxisomal acyl-coenzyme A oxidase 1; AST, aspartate aminotransferase; CCL, chemokine (C–C motif) ligand; CHOP, C/EBP homologous protein; cGAS, cyclic GMP–AMP synthase; COL1A, collagen 1 alpha; CPT1A, carnitine palmitoyl transferase 1 alpha; FASN, fatty acid synthase; FGF21, fibroblast growth factor 21; G6PC, glucose-6-phosphatase, catalytic subunit; MGST1, microsomal glutathione S-transferase 1; GPX2, glutathione peroxidase 2; GSTA2, glutathione S-transferase alpha 2; GSTM2, glutathione S-transferase mu 2; GSTT1, glutathione S-transferase theta 1; HMOX1, heme oxygenase 1; ICAM-1, intercellular adhesion molecule-1; KEAP1, kelch-like ECH-associated protein 1; LDH, lactate dehydrogenase; MAFLD, metabolic-associated fatty liver disease; NASH, nonalcoholic steatohepatitis; NFE2L2/NRF2, nuclear factor (erythroid-derived 2)-like 2; NFκB, nuclear factor kappa-light-chain-enhancer of activated B cells; NQO1, NAD(P)H quinone dehydrogenase 1; PCLS, precision cut liver slices; p-H2A.X,

phospho-Histone H2A.X PDK4, pyruvate dehydrogenase kinase 4; PPAR, peroxisome proliferator-activated receptor; ROS, reactive oxygen species; SOD, Superoxide Dismutase; SREBF1, sterol regulatory element binding transcription factor 1; STING, stimulator of interferon genes; TNFA, tumour necrosis factor alpha; VCAM-1, vascular cell adhesion molecule-1; XRCC1, X-ray repair cross complementing 1.

Financial support
RHU QUID-NASH is funded by Agence Nationale de la Recherche (ANR-17-RHUS-0009); implemented by Inserm, Université Paris Cité, CNRS, CEA, Laboratoires Servier, Biopredictive, and AP-HP; and coordinated by Prof. Dominique Valla and Angélique Brzustowski.

Conflicts of interest
AH was a post-doctoral researcher at Servier and Inserm. PD and NP are employees of Servier.

Please refer to the accompanying ICMJE disclosure forms for further details.

Authors' contributions
Designed the project and experiments and wrote the manuscript: AH, NP, PD, VP. Performed the experiments: AH, SL, NC. Performed the histological stainings and quantitative analyses: MA. Discussed and critically revised the manuscript: all authors.

Data availability statement
The data that support the findings of this study are available from the corresponding author upon reasonable request.

Acknowledgements
We thank members of the RHU QUID NASH consortium for their helpful discussions and their critical revision of the manuscript. We thank Agnès Dauvergne and Claude Hercend from the Clinical Biochemistry department of Beaujon Hospital, Clichy, France, for their help and advice on biochemical measurements in PCLS' culture supernatants. We are thankful to the iGenSeq core facility, Institut du Cerveau (Paris, France), and JR Analytics technology (jr-analytics.fr) for sharing their expertise and helping us with RNA sequencing analyses.

Supplementary data
Supplementary data to this article can be found online at https://doi.org/10.1016/j.jhepr.2023.100845.

References
Author names in bold designate shared co-first authorship.

[1] Karlsen TH, Sheron N, Zelber-Sagi S, Carrieri P, Dusheiko G, Bugianesi E, et al. The EASL-Lancet Liver Commission: protecting the next generation of Europeans against liver disease complications and premature mortality. Lancet Lond Engl 2022;399:61–116.
[2] Younossi Z, Anstee QM, Marietti M, Hardy T, Henry L, Eslam M, et al. Global burden of NAFLD and NASH: trends, predictions, risk factors and prevention. Nat Rev Gastroenterol Hepatol 2018;15:11–20.
[3] Estes C, Razavi H, Loomba R, Younossi Z, Sanyal AJ. Modeling the epidemic of nonalcoholic fatty liver disease demonstrates an exponential increase in burden of disease. Hepatology 2018;67:123–133.
[4] Eslam M, Sanyal AJ, George J, International Consensus Panel. MAFLD: a consensus-driven proposed nomenclature for metabolic associated fatty liver disease. Gastroenterology 2020;158:1999–2014.e1.
[5] Friedman SL, Neuschwander-Tetri BA, Rinella M, Sanyal AJ. Mechanisms of NAFLD development and therapeutic strategies. Nat Med 2018;24:908–922.
[6] Younossi ZM, Golabi P, de Avila L, Paik JM, Srishord M, Fukui N, et al. The global epidemiology of NAFLD and NASH in patients with type 2 diabetes: a systematic review and meta-analysis. J Hepatol 2019;71:793–801.
[7] Chalasani N, Younossi Z, Lavine JE, Charlton M, Cusi K, Rinella M, et al. The diagnosis and management of nonalcoholic fatty liver disease: practice guidance from the American Association for the Study of Liver Diseases. Hepatology 2018;67:328–357.
[8] **Loomba R**, **Friedman SL**, **Shulman GI**. Mechanisms and disease consequences of nonalcoholic fatty liver disease. Cell 2021;184:2537–2564.
[9] Huang DQ, El-Serag HB, Loomba R. Global epidemiology of NAFLD-related HCC: trends, predictions, risk factors and prevention. Nat Rev Gastroenterol Hepatol 2021;18:223–238.
[10] Younossi ZM. Non-alcoholic fatty liver disease – a global public health perspective. J Hepatol 2019;70:531–544.
[11] Vuppalanchi R, Noureddin M, Alkhouri N, Sanyal AJ. Therapeutic pipeline in nonalcoholic steatohepatitis. Nat Rev Gastroenterol Hepatol 2021;18:373–392.
[12] Cichoż-Lach H, Michalak A. Oxidative stress as a crucial factor in liver diseases. World J Gastroenterol 2014;20:8082–8091.
[13] Masarone M, Rosato V, Dallio M, Gravina AG, Aglitti A, Loguercio C, et al. Role of oxidative stress in pathophysiology of nonalcoholic fatty liver disease. Oxid Med Cel Longev 2018;2018:9547613.
[14] Madan K, Bhardwaj P, Thareja S, Gupta SD, Saraya A. Oxidant stress and antioxidant status among patients with nonalcoholic fatty liver disease (NAFLD). J Clin Gastroenterol 2006;40:930–935.
[15] Palmieri VO, Grattagliano I, Portincasa P, Palasciano G. Systemic oxidative alterations are associated with visceral adiposity and liver steatosis in patients with metabolic syndrome. J Nutr 2006;136:3022–3026.
[16] Mohs A, Otto T, Schneider KM, Peltzer M, Boekschoten M, Holland CH, et al. Hepatocyte-specific NRF2 activation controls fibrogenesis and carcinogenesis in steatohepatitis. J Hepatol 2021;74:638–648.
[17] Videla LA, Rodrigo R, Orellana M, Fernandez V, Tapia G, Quiñones L, et al. Oxidative stress-related parameters in the liver of non-alcoholic fatty liver disease patients. Clin Sci Lond Engl 1979 2004;106:261–268.
[18] Dodson M, de la Vega MR, Cholanians AB, Schmidlin CJ, Chapman E, Zhang DD. Modulating NRF2 in disease: timing is everything. Annu Rev Pharmacol Toxicol 2019;59:555–575.
[19] Tong KI, Katoh Y, Kusunoki H, Itoh K, Tanaka T, Yamamoto M. Keap1 recruits Neh2 through binding to ETGE and DLG motifs: characterization of the two-site molecular recognition model. Mol Cell Biol 2006;26:2887–2900.
[20] **Tong KI**, **Padmanabhan B**, Kobayashi A, Shang C, Hirotsu Y, Yokoyama S, et al. Different electrostatic potentials define ETGE and DLG motifs as hinge and latch in oxidative stress response. Mol Cell Biol 2007;27:7511–7521.
[21] Bellezza I, Giambanco I, Minelli A, Donato R. Nrf2-Keap1 signaling in oxidative and reductive stress. Biochim Biophys Acta Mol Cell Res 2018;1865:721–733.
[22] Hayes JD, Dinkova-Kostova AT. The Nrf2 regulatory network provides an interface between redox and intermediary metabolism. Trends Biochem Sci 2014;39:199–218.
[23] Tang W, Jiang Y-F, Ponnusamy M, Diallo M. Role of Nrf2 in chronic liver disease. World J Gastroenterol 2014;20:13079–13087.
[24] **Xu D**, **Xu M**, Jeong S, Qian Y, Wu H, Xia Q, et al. The Role of Nrf2 in liver disease: novel molecular mechanisms and therapeutic approaches. Front Pharmacol 2018;9:1428.
[25] Bricambert J, Alves-Guerra M-C, Esteves P, Prip-Buus C, Bertrand-Michel J, Guillou H, et al. The histone demethylase Phf2 acts as a molecular checkpoint to prevent NAFLD progression during obesity. Nat Commun 2018;9:2092.
[26] **Azzimato V**, **Jager J**, **Chen P**, Morgantini C, Levi L, Barreby E, et al. Liver macrophages inhibit the endogenous antioxidant response in obesity-associated insulin resistance. Sci Transl Med 2020;12:eaaw9709.
[27] Tanaka Y, Aleksunes LM, Yeager RL, Gyamfi MA, Esterly N, Guo GL, et al. NF-E2-related factor 2 inhibits lipid accumulation and oxidative stress in mice fed a high-fat diet. J Pharmacol Exp Ther 2008;325:655–664. https://doi.org/10.1124/jpet.107.135822.
[28] Chowdhry S, Nazmy MH, Meakin PJ, Dinkova-Kostova AT, Walsh SV, Tsujita T, et al. Loss of Nrf2 markedly exacerbates nonalcoholic steatohepatitis. Free Radic Biol Med 2010;48:357–371. https://doi.org/10.1016/j.freeradbiomed.2009.11.007.
[29] Shimozono R, Asaoka Y, Yoshizawa Y, Aoki T, Noda H, Yamada M, et al. Nrf2 activators attenuate the progression of nonalcoholic steatohepatitis-related fibrosis in a dietary rat model. Mol Pharmacol 2013;84:62–70.
[30] Sharma RS, Harrison DJ, Kisielewski D, Cassidy DM, McNeilly AD, Gallagher JR, et al. Experimental nonalcoholic steatohepatitis and liver fibrosis are ameliorated by pharmacologic activation of Nrf2 (NF-E2 p45-Related Factor 2). Cell Mol Gastroenterol Hepatol 2018;5:367–398.
[31] Li X, Zhang D, Hannink M, Beamer LJ. Crystal structure of the Kelch domain of human Keap1. J Biol Chem 2004;279:54750–54758.
[32] Schmoll D, Engel CK, Glombik H. The Keap1-Nrf2 protein-protein interaction: a suitable target for small molecules. Drug Discov Today Technol 2017;24:11–17.

[33] **Davies TG**, **Wixted WE**, Coyle JE, Griffiths-Jones C, Hearn K, McMenamin R, et al. Monoacidic inhibitors of the Kelch-like ECH-associated protein 1: nuclear factor erythroid 2-related factor 2 (KEAP1:NRF2) protein-protein interaction with high cell potency identified by fragment-based discovery. J Med Chem 2016;59:3991–4006.

[34] **Seedorf K**, **Weber C**, Vinson C, Berger S, Vuillard L-M, Kiss A, et al. Selective disruption of NRF2-KEAP1 interaction leads to NASH resolution and reduction of liver fibrosis in mice. JHEP Rep 2022;5:100651.

[35] Palma E, Doornebal EJ, Chokshi S. Precision-cut liver slices: a versatile tool to advance liver research. Hepatol Int 2019;13:51–57.

[36] Staels B, Rubenstrunk A, Noel B, Rigou G, Delataille P, Millatt LJ, et al. Hepatoprotective effects of the dual peroxisome proliferator-activated receptor alpha/delta agonist, GFT505, in rodent models of nonalcoholic fatty liver disease/nonalcoholic steatohepatitis. Hepatology 2013;58:1941–1952.

[37] Ratziu V, Harrison SA, Francque S, Bedossa P, Lehert P, Serfaty L, et al. Elafibranor, an agonist of the peroxisome proliferator-activated receptor-α and -δ, induces resolution of nonalcoholic steatohepatitis without fibrosis worsening. Gastroenterology 2016;150:1147–1159.e5.

[38] Perakakis N, Stefanakis K, Feigh M, Veidal SS, Mantzoros CS. Elafibranor and liraglutide improve differentially liver health and metabolism in a mouse model of non-alcoholic steatohepatitis. Liver Int 2021;41:1853–1866.

[39] de Graaf IAM, Olinga P, de Jager MH, Merema MT, de Kanter R, van de Kerkhof EG, et al. Preparation and incubation of precision-cut liver and intestinal slices for application in drug metabolism and toxicity studies. Nat Protoc 2010;5:1540–1551.

[40] Paish HL, Reed LH, Brown H, Bryan MC, Govaere O, Leslie J, et al. A bioreactor technology for modeling fibrosis in human and rodent precision-cut liver slices. Hepatology 2019;70:1377–1391.

[41] Lagaye S, Shen H, Saunier B, Nascimbeni M, Gaston J, Bourdoncle P, et al. Efficient replication of primary or culture hepatitis C virus isolates in human liver slices: a relevant ex vivo model of liver infection. Hepatology 2012;56:861–872.

[42] Boeckmans J, Buyl K, Natale A, Vandenbempt V, Branson S, De Boe V, et al. Transcriptomics data of a human in vitro model of non-alcoholic steatohepatitis exposed to elafibranor. Data Brief 2019;25:104093.

[43] Tanaka S, Miyanishi K, Kobune M, Kawano Y, Hoki T, Kubo T, et al. Increased hepatic oxidative DNA damage in patients with nonalcoholic steatohepatitis who develop hepatocellular carcinoma. J Gastroenterol 2013;48:1249–1258.

[44] Clutton S. The importance of oxidative stress in apoptosis. Br Med Bull 1997;53:662–668.

[45] Wang JY. DNA damage and apoptosis. Cell Death Differ 2001;8:1047–1048.

[46] Chen R, Du J, Zhu H, Ling Q. The role of cGAS-STING signalling in liver diseases. JHEP Rep Innov Hepatol 2021;3:100324.

[47] **Luo X**, **Li H**, **Ma L**, Zhou J, Guo X, Woo S-L, et al. Expression of STING is increased in liver tissues from patients with NAFLD and promotes macrophage-mediated hepatic inflammation and fibrosis in mice. Gastroenterology 2018;155:1971–1984.e4.

[48] Risérus U, Sprecher D, Johnson T, Olson E, Hirschberg S, Liu A, et al. Activation of peroxisome proliferator-activated receptor (PPAR)delta promotes reversal of multiple metabolic abnormalities, reduces oxidative stress, and increases fatty acid oxidation in moderately obese men. Diabetes 2008;57:332–339.

[49] Allaire M, Rautou P-E, Codogno P, Lotersztajn S. Autophagy in liver diseases: time for translation? J Hepatol 2019;70:985–998.

[50] Hammoutene A, Biquard L, Lasselin J, Kheloufi M, Tanguy M, Vion A-C, et al. A defect in endothelial autophagy occurs in patients with non-alcoholic steatohepatitis and promotes inflammation and fibrosis. J Hepatol 2020;72:528–538.

[51] Zhang X-Q, Xu C-F, Yu C-H, Chen W-X, Li Y-M. Role of endoplasmic reticulum stress in the pathogenesis of nonalcoholic fatty liver disease. World J Gastroenterol 2014;20:1768–1776.

[52] Mizushima N, Yoshimori T. How to interpret LC3 immunoblotting. Autophagy 2007;3:542–545.

[53] Hammoutene A, Rautou P-E. Role of liver sinusoidal endothelial cells in non-alcoholic fatty liver disease. J Hepatol 2019;70:1278–1291.

[54] Dewyse L, Reynaert H, van Grunsven LA. Best practices and progress in precision-cut liver slice cultures. Int J Mol Sci 2021;22:7137.

[55] Lonardo A, Nascimbeni F, Ballestri S, Fairweather D, Win S, Than TA, et al. Sex differences in nonalcoholic fatty liver disease: state of the art and identification of research gaps. Hepatology 2019;70:1457–1469.

[56] Castera L, Laouenan C, Vallet-Pichard A, Vidal-Trécan T, Manchon P, Paradis V, et al. High prevalence of NASH and advanced fibrosis in type 2 diabetes: a prospective study of 330 outpatients undergoing liver biopsies for elevated ALT, using a low threshold. Diabetes Care 2023;46:1354–1362.

[57] van den Hoek AM, Verschuren L, Caspers MPM, Worms N, Menke AL, Princen HMG. Beneficial effects of elafibranor on NASH in E3L.CETP mice and differences between mice and men. Sci Rep 2021;11:5050.

[58] Yates MS, Tran QT, Dolan PM, Osburn WO, Shin S, McCulloch CC, et al. Genetic versus chemoprotective activation of Nrf2 signaling: overlapping yet distinct gene expression profiles between Keap1 knockout and triterpenoid-treated mice. Carcinogenesis 2009;30:1024–1031.

[59] Chambel SS, Santos-Gonçalves A, Duarte TL. The dual role of Nrf2 in nonalcoholic fatty liver disease: regulation of antioxidant defenses and hepatic lipid metabolism. Biomed Res Int 2015;2015:597134.

[60] Luedde T, Beraza N, Kotsikoris V, van Loo G, Nenci A, De Vos R, et al. Deletion of NEMO/IKKgamma in liver parenchymal cells causes steatohepatitis and hepatocellular carcinoma. Cancer Cell 2007;11:119–132.

[61] Wani WY, Boyer-Guittaut M, Dodson M, Chatham J, Darley-Usmar V, Zhang J. Regulation of autophagy by protein post-translational modification. Lab Investig J Tech Methods Pathol 2015;95:14–25.

[62] Nishida N, Yada N, Hagiwara S, Sakurai T, Kitano M, Kudo M. Unique features associated with hepatic oxidative DNA damage and DNA methylation in non-alcoholic fatty liver disease. J Gastroenterol Hepatol 2016;31:1646–1653.

[63] Donne R, Saroul-Ainama M, Cordier P, Hammoutene A, Kabore C, Stadler M, et al. Replication stress triggered by nucleotide pool imbalance drives DNA damage and cGAS-STING pathway activation in NAFLD. Dev Cell 2022;57:1728–1741.

[64] Guicciardi ME, Gores GJ. Apoptosis: a mechanism of acute and chronic liver injury. Gut 2005;54:1024–1033.

[65] Kaina B. DNA damage-triggered apoptosis: critical role of DNA repair, double-strand breaks, cell proliferation and signaling. Biochem Pharmacol 2003;66:1547–1554.

[66] **Wang P**, **Ni M**, **Tian Y**, Wang H, Qiu J, You W, et al. Myeloid Nrf2 deficiency aggravates non-alcoholic steatohepatitis progression by regulating YAP-mediated NLRP3 inflammasome signaling. iScience 2021;24:102427.

[67] Wardyn JD, Ponsford AH, Sanderson CM. Dissecting molecular cross-talk between Nrf2 and NF-κB response pathways. Biochem Soc Trans 2015;43:621–626.

[68] Tølbøl KS, Kristiansen MN, Hansen HH, Veidal SS, Rigbolt KT, Gillum MP, et al. Metabolic and hepatic effects of liraglutide, obeticholic acid and elafibranor in diet-induced obese mouse models of biopsy-confirmed nonalcoholic steatohepatitis. World J Gastroenterol 2018;24:179–194.

[69] Zheng H, Whitman SA, Wu W, Wondrak GT, Wong PK, Fang D, et al. Therapeutic potential of Nrf2 activators in streptozotocin-induced diabetic nephropathy. Diabetes 2011;60:3055–3066.

[70] Prestigiacomo V, Suter-Dick L. Nrf2 protects stellate cells from Smad-dependent cell activation. PLoS One 2018;13:e0201044.

Journal of Hepatology, Volume *5*

Supplemental information

A new NRF2 activator for the treatment of human metabolic dysfunction-associated fatty liver disease

Adel Hammoutene, Samira Laouirem, Miguel Albuquerque, Nathalie Colnot, Angélique Brzustowski, Dominique Valla, Nicolas Provost, Philippe Delerive, Valérie Paradis, and on behalf of the QUID-NASH Research Group

A new NRF2 activator for the treatment of human metabolic dysfunction-associated fatty liver disease

Adel Hammoutene[1,2], Samira Laouirem[1], Miguel Albuquerque[1,3], Nathalie Colnot[3], Angélique Brzustowski[1], Dominique Valla[1], Nicolas Provost[2], Philippe Delerive[2], Valérie Paradis[1,3], on behalf of the QUID-NASH research group

Table of contents

QUID-NASH Research Group members 2
Supplementary material and methods 3
ATP content determination 3
RNA extraction and quantitative polymerase chain reaction 3
Western blot 3
Triglyceride and GSH contents determination 4
Histopathology and immunohistochemistry 4
Culture supernatants preparation and biochemical measurements 5
Transcriptomic analysis 5
Supplementary Figures 7
Fig. S1 7
Fig. S2 8
Fig. S3 9
Fig. S4 10
Fig. S5 11
Fig. S6 12
Fig. S7 14
Fig. S8 16
Fig. S9 17
Supplementary Tables 19
Table S1 19
Table S2 20
Table S3 21
Table S4 22
Table S5 23
Table S6 ..... Excel
References 24

QUID-NASH Research Group members

QUID-NASH project coordinators: Prof. Dominique Valla & Angélique Brzustowski

Beaujon hospital group (Université de Paris, Assistance Publique-Hôpitaux de Paris and Inserm CRI-UMR1149): Laurent Castéra, Pierre-Emmanuel Rautou, Bernard Van Beers, Valérie Vilgrain, Philippe Garteiser, Marco Diogardi-Burbio, Sabrina Doblas, Valérie Paradis, Pierre Bedossa, Miguel Albuquerque and Adel Hammoutene

Lariboisière hospital group (Université de Paris, Assistance Publique-Hôpitaux de Paris and Inserm U1138**:** Jean-François Gautier, Tiphaine Vidal-Trécan, Jean-Pierre Riveline, Jean-Baptiste Julla.

Cochin hospital group (Université de Paris, Assistance Publique-Hôpitaux de Paris and Institut Cochin): Christian Boitard, Etienne Larger, Stanislas Pol, Anaïs Vallet-Pichard, Benoît Terris, Béatrice Parfait, Catherine Postic, Agnès Lehuen, Amine Toubal, Camille Rousseau, Blandine Fruchet, Pauline Soulard, Zouriatou Gouda, Michel Vidaud, Franck Letourneur, Gilles Renault, Raphaël Scharfmann

Necker-Enfants Malades hospital group (Université de Paris, Assistance Publique-Hôpitaux de Paris): Jean-Michel Corréas

European hospital George Pompidou research group (Université de Paris, Assistance Publique-Hôpitaux de Paris and Inserm UMR1153**)**: Sébastien Czernichow, Claire Carette, Charles Barsamian

Avicenne hospital group (Université Paris 13, Assistance publique-Hôpitaux de Paris and Inserm U955, Université Paris-Est, Créteil): Dominique Roulot-Marullo, Hélène Bihan, Emmanuel Cosson

Physics for Medicine Paris group (Inserm, CNRS and Ecole supérieur de Physique et Chimie de Paris ESPCI): Mickael Tanter, Thomas Deffieux, Sofiane Decombas, Thu-mai Nguyen

Biomedical imagery lab group (Inserm, Sorbonne Université and CNRS): Olivier Couture, Rachel Baida

Département d'Epidémiologie, Biostatistiques et Recherche Clinique HUPNVS (Université de Paris, Assistance Publique-Hôpitaux de Paris Inserm IAME-UMR1137 and URC PNVS): Cédric Laouénan, Jimmy Mullaert, Delphine Bachelet, Nathalie Gault, Estelle Marcault, Nassima Si-Mohammed, Pauline Manchon, Basma Basli-Baillet, Krishna Bhavsar

Unité de Recherche clinique en Economie de la Santé – Ile de France (URC-Eco) (Université Paris 12, Assistance Publique-Hôpitaux de Paris): Isabelle Durand Zaleski

Servier group: Nathalie de Préville, Philippe Delerive, Tania Baltauss, Erwan Werner, Laura Xuereb, Julia Geronimi, Jessica Laplume, Valérie Duvivier, Pierre Barbier Saint Hilaire, Edwige-Ludiwyne Balzac

Swiss Institute of Bioinformatics group: Mark Ibberson, Olivier Martin, Manuela Pruess

BioPrédictive: Thierry Poynard, Olivier Deckmyn

Commissariat à l'Energie Atomique: Christophe Junot, François Fenaille, Florence Castelli, Benoit Colsch

Supplementary material and methods

ATP content determination: PCLS viability was in part assessed *via* ATP content determination as described below [1]. Briefly, PCLS were homogenized in 500 µL of 2 mmol/L EDTA - 70% ethanol solution (pH 10.9) using a TissueLyser LT (Qiagen). ATP content was determined using the bioluminescent CellTiter-Glo® 3D Cell Viability Assay (Promega G9681) according to the manufacturer's instructions. Luminescence was recorded with a Fluoroskan FL microplate reader (ThermoFisher Scientific). ATP content was normalized to total protein content of the slice as measured by the Bradford Protein Assay (Bio-Rad). Presented results are expressed as the mean of the two slices for each condition.

RNA extraction and quantitative polymerase chain reaction: mRNA from PCLS were extracted in TRIzol® reagent (Life technologies) according to manufacturers' instructions. cDNA synthesis was performed with QuantiTect Reverse Transcription Kit (Qiagen). Quantitative polymerase chain reaction (qPCR) was performed on Real-Time PCR system LightCycler® 96 Instrument (Roche) using TaqMan® probes (Appliedbiosystems) with the following parameters: 1 cycle at 95°C for 10 min followed by 45 cycles at 95°C for 15s, 60°C for 60s. Probes references are detailed in Table S4. Gene expression was normalized to four housekeeping genes (*18s*, *GAPDH, HPRT1* and *PPIA*). Relative expression was calculated using the 2-delta-delta CT method and geometric average of normalization to each housekeeping gene was calculated. Presented results are expressed as the mean of the two slices for each condition.

Western blot: Snap frozen PCLS were homogenized in 200 µL RIPA buffer containing 150 mmol/L NaCl, 50 mmol/L TrisHCl, pH 7.4, 2 mmol/L EDTA, 0.5% sodium deoxycholate, 0.2% sodium dodecyl sulfate, 2 mmol/L activated orthovanadate, complete protease inhibitor cocktail tablet (cOmplete™, Roche) and complete phosphatase inhibitor cocktail tablet (PhosSTOP™, Roche). Homogenates were then incubated at 4°C for 45 minutes. Lysates were centrifuged at 12000 g for 5 min. Supernatants were collected and protein content was

quantified using the Lowry protein assay (Bio-Rad; Hercules, CA). Lysates were mixed with the reducing sample buffer for electrophoresis and subsequently transferred onto nitrocellulose membrane (Bio-Rad). Equal loading was checked using Ponceau red solution. Membranes were incubated with primary antibodies (primary antibodies used for western blot analyses are described in Table S5). After secondary antibody incubation (anti-rabbit or anti-mouse, Amersham, GE Healthcare, 1/3000), immunodetection was performed using an enhanced chemiluminescence kit (Immun-Star Western C kit, Bio-Rad). Bands were revealed using the ChemiDoc imaging system (Bio-Rad). Values reported from Western blots were obtained by band density analysis using Image Lab software (Bio-Rad) and expressed as the ratio of protein of interest on total loaded proteins (ponceau) for the whole cell extract.

Triglyceride and GSH contents determination: Snap frozen PCLS were homogenized in 500 μL PBS using a TissueLyser LT (Qiagen). Triglyceride content was determined using the bioluminescent Triglyceride-Glo™ Assay (Promega J3160) and GSH content was determined using the GSH-Glo™ Glutathione Assay (Promega V6911) according to the manufacturer's instructions. Luminescence was recorded with a Fluoroskan FL microplate reader (ThermoFisher Scientific). Triglyceride and GSH contents were normalized to total protein content of the slice as measured by the Bradford Protein Assay (Bio-Rad).

Histopathology and immunohistochemistry: PCLS were fixed in 10% formalin for 24 hours and embedded in paraffin with an automated carousel processor for dehydration, and paraffin embedding (Leica). Histopathology and immunostainings were performed using standard clinical procedures in the Pathology department of Beaujon Hospital (Clichy, France). Briefly, 3 μm thickness sections were made and stained with Hematoxylin and Eosin or Sirius red. Immunostainings for alpha-smooth muscle actin (α-SMA), CD68, phospho-Histone H2A.X (p-H2A.X) and cleaved Caspase-3 were performed with an automated immunohistochemical stainer (Ventana Benchmark®) according to the manufacturer's instructions (primary antibodies used for immunohistochemistry analyses are described in Table S5). Stained and immunostained slides were digitized (Scanscope AT turbo®, Leica). Steatosis was scored on

Hematoxylin and Eosin staining by a pathologist (VP) in a blinded manner, according to the following scoring system that assesses the proportion of large or medium fat droplets containing hepatocytes: S0: <5%; S1: 5–33%; S2: 34–66%; S3: >67% [2]. Quantitative analyses of immunostainings (α-SMA, cleaved Caspase-3 and CD68) and sirius red staining was performed using positive pixels algorithm (Indica Labs) on digital slides with Aperio software. Results are expressed as the percentage of positive pixels. p-H2A.X immunostaining analysis was performed using positive cells algorithm on digital slides with Qupath software and expressed as the percentage of positive nuclei. Quantification methods were automated observer-independent process based on whole-slide scanning.

Culture supernatants preparation and biochemical measurements: PCLS culture supernatants were collected after the 48th hour of culture and centrifuged for 15 minutes at 600g in order to remove cell debris. Supernatants were aliquoted and stored at -80°C until use. Aspartate aminotransferase (AST) level were measured by colorimetric assay (Cohesion Biosources CAK1004) according to the manufacturer's instructions. Absorbance at 520 nm was recorded with a Multiskan sky microplate reader (ThermoFisher Scientific). LDH and glucose levels were measured in PCLS supernatants by standard clinical procedures at Beaujon Hospital (Clichy, France).

Transcriptomic analysis: mRNA from PCLS were extracted in TRIzol® reagent reagent (Life technologies) according to manufacturer's instructions. To monitor modulated genes following Elafibranor or S217879 treatments, an RNA library was prepared using the SMARTer® Stranded Total RNA-Seq Kit v3 (Pico Input Mammalian) according to manufacturer's recommendations (634873, Takara). Samples were sequenced on ILLUMINA Novaseq 6000 with S1-200 cartridge in the iGenSeq core facility (Genotyping and sequencing), at Institut du Cerveau (Paris, France). Raw RNA-seq reads were mapped to the human genome (Ensembl GRCH38) and Ensembl's reference transcriptome using STAR [3]. Gene counts were obtained using FeatureCount [4], normalized by an UpperQuartile procedure, and logged on a base 2. RNAseq analyses were performed by JR Analytics (jr-analytics.fr). Genes from sexual

chromosomes and genes with null variance were removed prior normalization. Raw Gene expression profiles were normalized using the upper-quartile approach and log2+1 transformed [5]. Analyses were corrected for gender effects. Differential gene expression between groups (Elafibranor *vs.* DMSO, and S217879 *vs.* DMSO, and Elafibranor *vs.* S217879) were estimated and the statistical relevance evaluated with Student's t test. Gene set enrichment analysis (GSEA) was performed using the fast GSEA implementation (10.18129/B9.bioc.fgsea; Bioconductor, open-source software), preranked by the t.test value from the studied comparison. Leading edges of gene set enrichment (genes having the most impact in the enrichment pathway) were displayed as a heatmaps.

RNA sequencing data presented here have been deposited in NCBI's Gene Expression Omnibus and are accessible through GEO Series accession number GSE234415 (https://www.ncbi.nlm.nih.gov/geo/query/acc.cgi?acc=GSE234415).

Supplementary figures

Figure S1

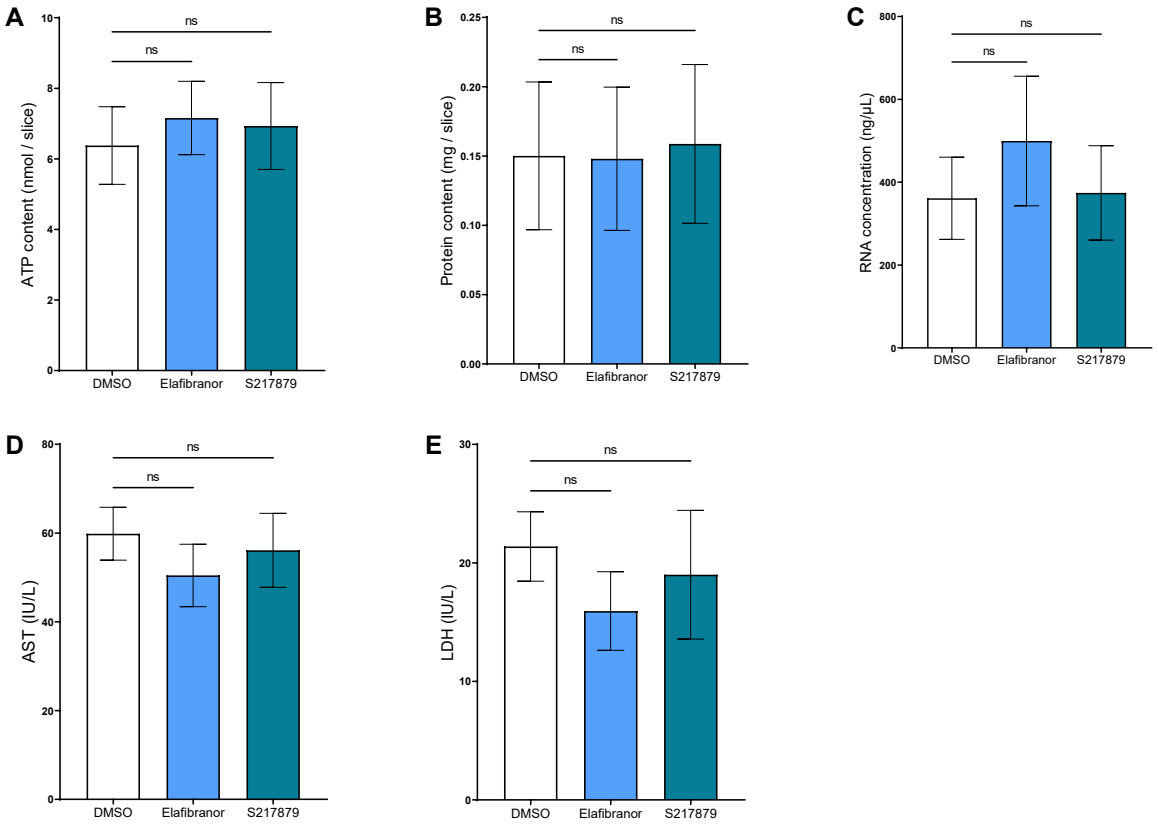

Fig. S1: Drugs safety. Human PCLS were generated from the liver of patients with MAFLD and treated with Elafibranor (10 µM) or S217879 (3 µM) or vehicle (DMSO, 0.1%) for two days. (**A**) Quantification of ATP, (**B**) protein and (**C**) RNA contents in human PCLS with MAFLD. (**D**) Quantification of AST and (**D**) LDH levels in PCLS culture supernatants. n=12 PCLS per condition generated from 12 patients with MAFLD. Data are expressed as mean ± SEM. ns, not significant (Wilcoxon paired t-test). MAFLD, metabolic associated fatty liver disease; PCLS, precision cut liver slices.

Figure S2

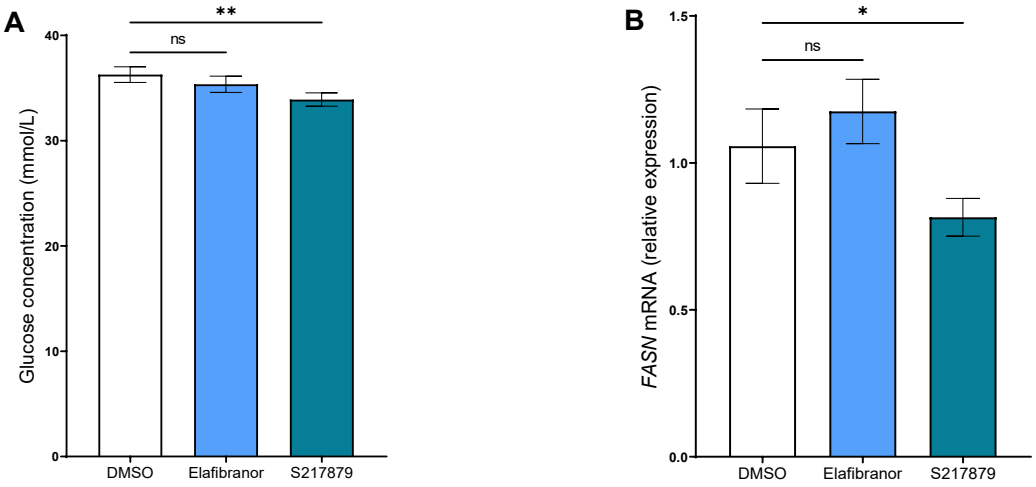

Fig. S2: S217879 but not Elafibranor inhibits neoglucogenesis and *de novo* lipogenesis. Human PCLS were generated from the liver of patients with MAFLD and treated with Elafibranor (10 µM) or S217879 (3 µM) or vehicle (DMSO, 0.1%) for two days. (**A**) Quantification of glucose concentration in PCLS culture supernatants. (**B**) qPCR analysis of *FASN* expression in human PCLS with MAFLD. n=12 PCLS per condition generated from 12 patients with MAFLD. Data are expressed as mean ± SEM. *p<0.05; **p<0.01; ns, not significant (Wilcoxon paired t-test). MAFLD, metabolic associated fatty liver disease; PCLS, precision cut liver slices.

Figure S3

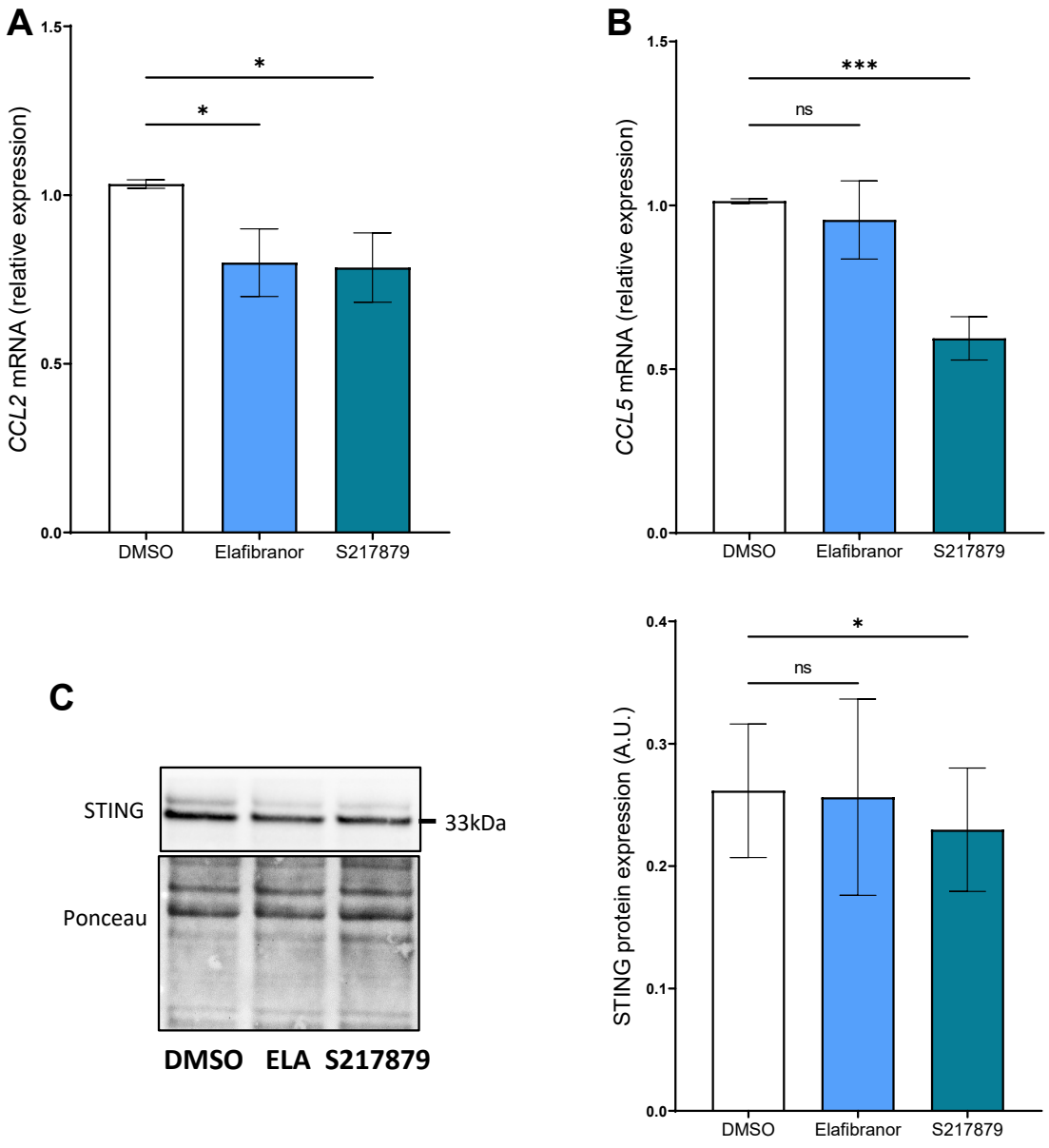

Fig. S3: Elafibranor and S217879 reduce liver inflammation. Human PCLS were generated from the liver of patients with MAFLD and treated with Elafibranor (10 µM) or S217879 (3 µM) or vehicle (DMSO, 0.1%) for two days. (**A**) qPCR analysis of *CCL2* and (**B**) *CCL5* expression in human PCLS with MAFLD. (**C**) Immunoblot analysis of STING expression in human PCLS with MAFLD. n=12 PCLS per condition generated from 12 patients with MAFLD. Data are expressed as mean ± SEM. *p<0.05; ***p<0.001; ns, not significant (Wilcoxon paired t-test). MAFLD, metabolic associated fatty liver disease; PCLS, precision cut liver slices.

Figure S4

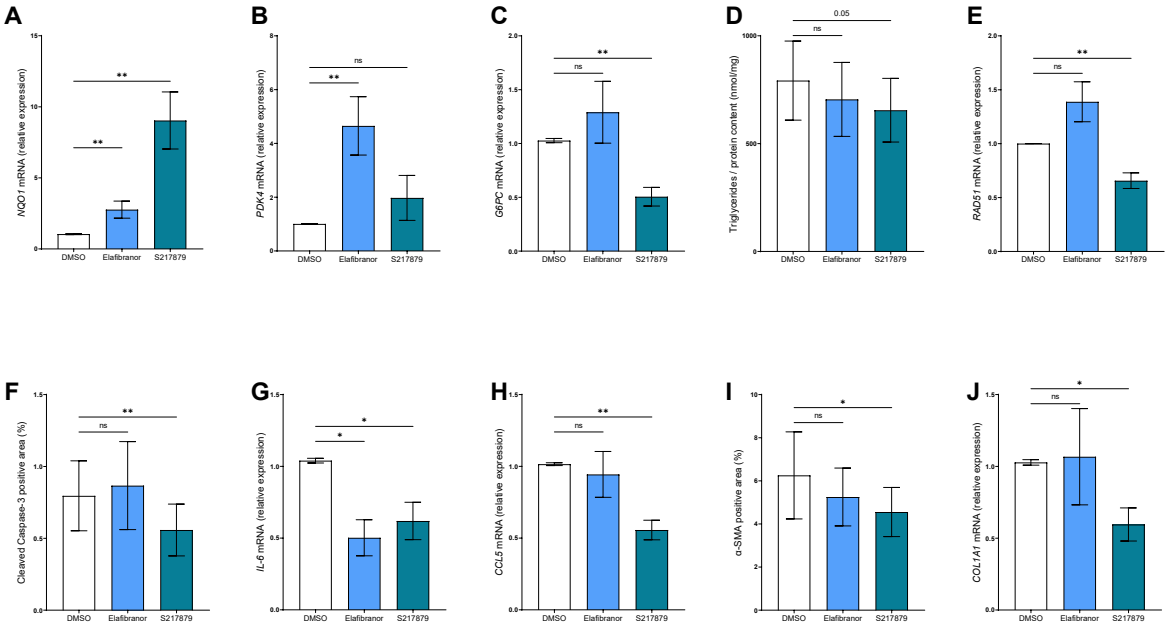

Fig. S4: Effects of Elafibranor and S217879 on PCLS from patients with advanced liver fibrosis. Human PCLS were generated from the liver of patients with MAFLD with advanced liver fibrosis (F3-F4, n=9 patients) and treated with Elafibranor (10 µM) or S217879 (3 µM) or vehicle (DMSO, 0.1%) for two days. qPCR analysis of *NQO1* (**A**), *PDK4* (**B**), and *G6PC* (**C**) expression in PCLS with MAFLD from patients with advanced liver fibrosis. (**D**) Quantification of triglycerides content (Triglycerides/protein content ratio) in PCLS with MAFLD from patients with advanced liver fibrosis. (**E**) qPCR analysis of *RAD51* expression in PCLS with MAFLD from patients with advanced liver fibrosis. (**F**) Immunohistochemical analysis of cleaved Caspase-3 positive area (%) on PCLS with MAFLD from patients with advanced liver fibrosis. (**G**) qPCR analysis of *IL-6* and (**H**) *CCL5* expression in PCLS with MAFLD from patients with advanced liver fibrosis. (**I**) Immunohistochemical analysis of α-SMA positive area (%) on PCLS with MAFLD from patients with advanced liver fibrosis. (**G**) qPCR analysis of *COL1A1* expression in PCLS with MAFLD from patients with advanced liver fibrosis. Data are expressed as mean ± SEM. *p<0.05; **p<0.01; ns, not significant (Wilcoxon paired t-test). Same patients were used in the analyses of drugs effects in patients with all stages of fibrosis (Figures 1-5, 7). MAFLD, metabolic associated fatty liver disease; PCLS, precision cut liver slices.

Figure S5

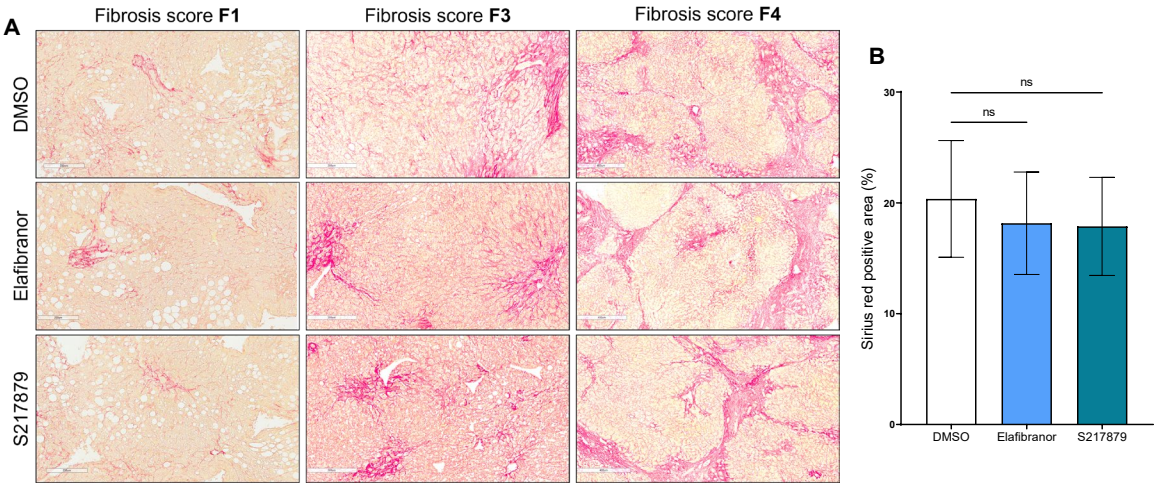

Fig. S5: Elafibranor and S217879 does not affect liver fibrosis. Human PCLS were generated from the liver of patients with MAFLD and treated with Elafibranor (10 µM) or S217879 (3 µM) or vehicle (DMSO, 0.1%) for two days. Fibrosis deposition was evaluated on Sirius red staining. (**A**) Representative images of histological analysis of liver fibrosis on Sirius red staining on PCLS sections from patients with F1, F3 or F4 fibrosis score [2]. (**B**) Quantification of liver fibrosis area on Sirius red stained slides. n=12 PCLS per condition generated from 12 patients with MAFLD. Data are expressed as mean ± SEM. ns, not significant (Wilcoxon paired t-test). MAFLD, metabolic associated fatty liver disease; PCLS, precision cut liver slices.

Figure S6

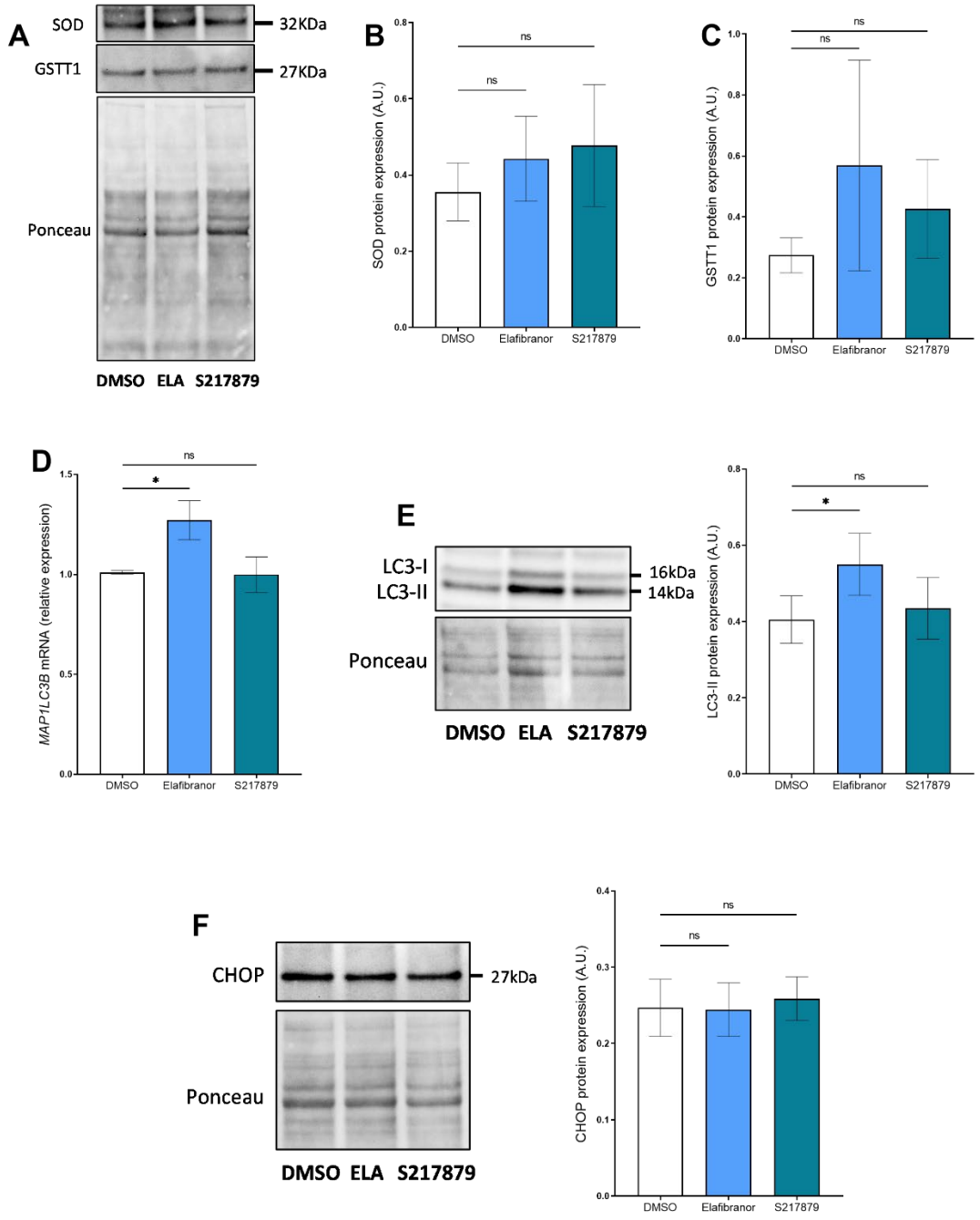

Fig. S6: Effects of Elafibranor and S217879 on liver autophagy and ER-stress. Human PCLS were generated from the liver of patients with MAFLD and treated with Elafibranor (10 µM) or S217879 (3 µM) or vehicle (DMSO, 0.1%) for two days. (**A**) Representative western blotting of SOD and GSTT1 expression. (**B**) Quantification of SOD and (**C**) GSTT1 protein expression. (**D**) qPCR analysis of LC3 expression (*MAP1LC3B*) in human PCLS with MAFLD. (**E**) Immunoblot analysis of LC3-II expression in human PCLS with MAFLD. (**F**) Immunoblot

analysis of CHOP expression in human PCLS with MAFLD. Data are expressed as mean ± SEM. n=12 PCLS per condition generated from 12 patients with MAFLD. *p<0.05; ns, not significant (Wilcoxon paired t-test). GSTT1, Glutathione S-Transferase Theta 1; MAFLD, metabolic associated fatty liver disease; PCLS, precision cut liver slices; SOD, superoxide dismutase.

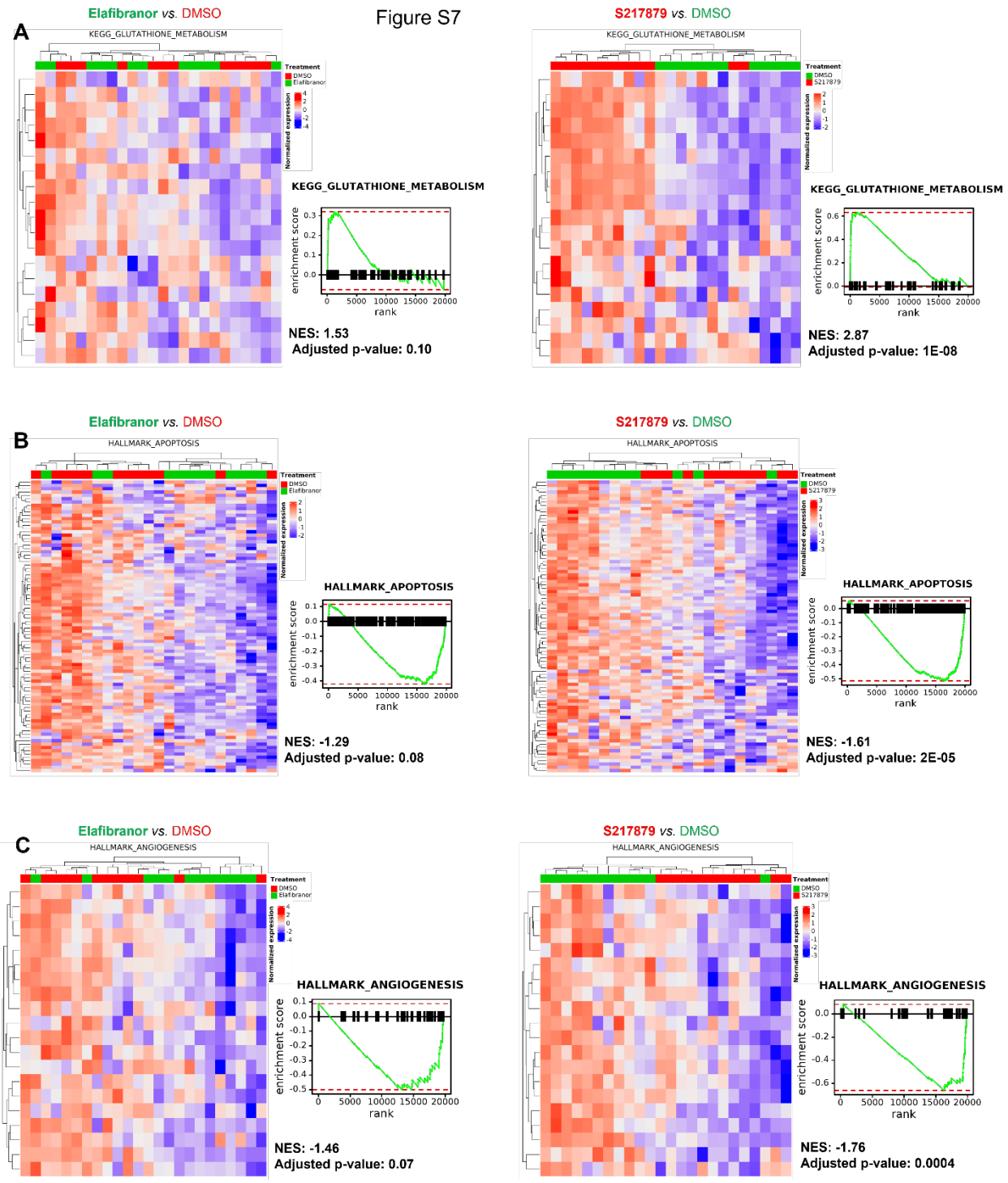

Fig. S7: S217879 treatment induces a potent anti-oxidant response and inhibits apoptosis and angiogenesis. Human PCLS were generated from the liver of patients with MAFLD and treated with Elafibranor (10 µM) or S217879 (3 µM) or vehicle (DMSO, 0.1%) for two days. (**A**) Heatmaps and enrichment plots of differentially expressed genes in glutathione metabolism, (**B**) apoptosis, and (**C**) angiogenesis pathways in Elafibranor and S217879-

treated PCLS *vs.* vehicle treated-PCLS. n=12 PCLS per condition generated from 12 patients with MAFLD. MAFLD, metabolic associated fatty liver disease; NES, normalized enrichment score; PCLS, precision cut liver slices.

Figure S8

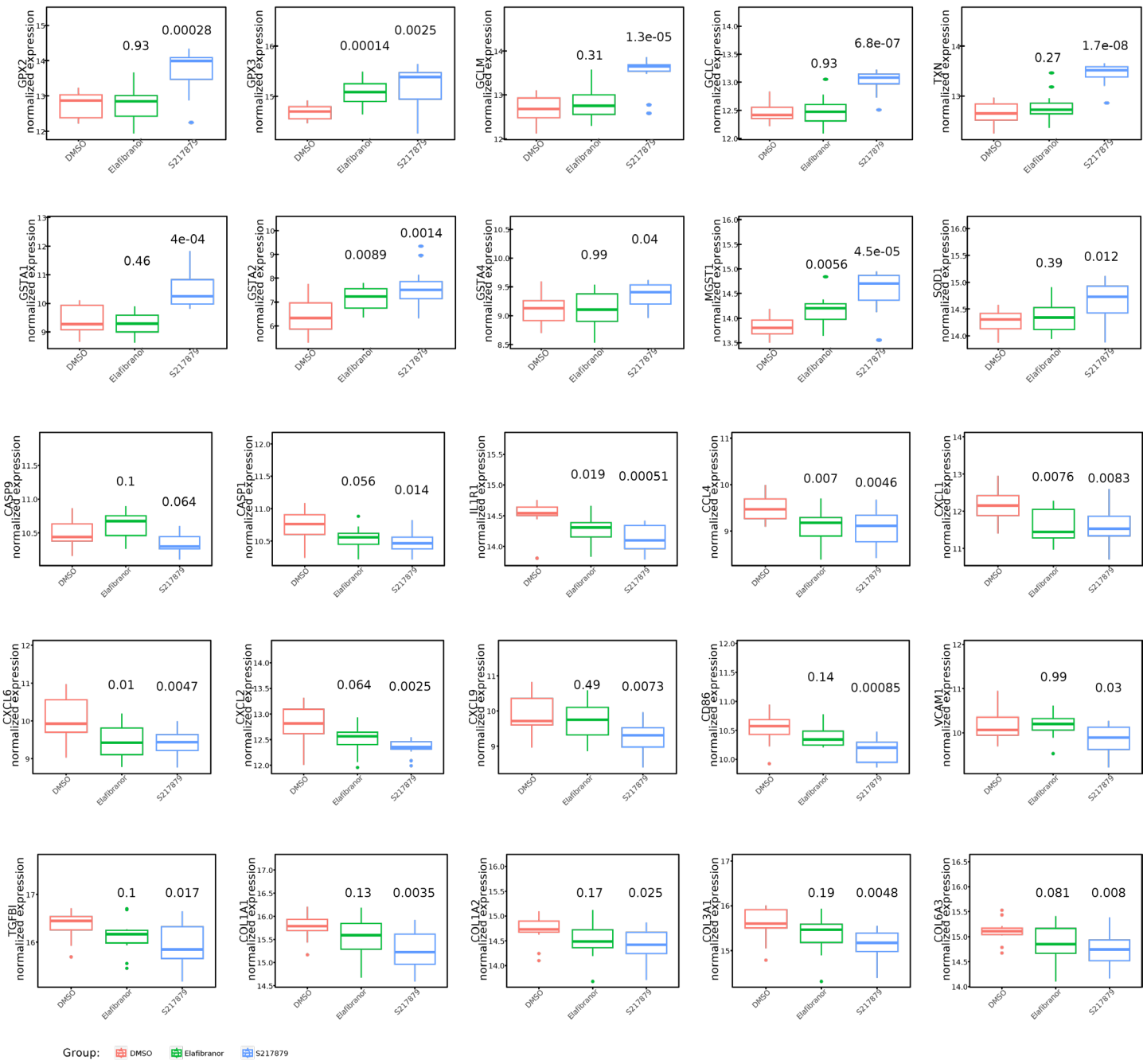

Fig. S8: Differentially expressed genes in Elafibranor and S217879-treated PCLS *vs.* vehicle-treated PCLS. Human PCLS were generated from the liver of patients with MAFLD and treated with Elafibranor (10 µM) or S217879 (3 µM) or vehicle (DMSO, 0.1%) for two days (n=12 PCLS per condition from 12 patients with MAFLD). Gene expression was evaluated on RNA sequencing data and are expressed as normalized counts.

Figure S9

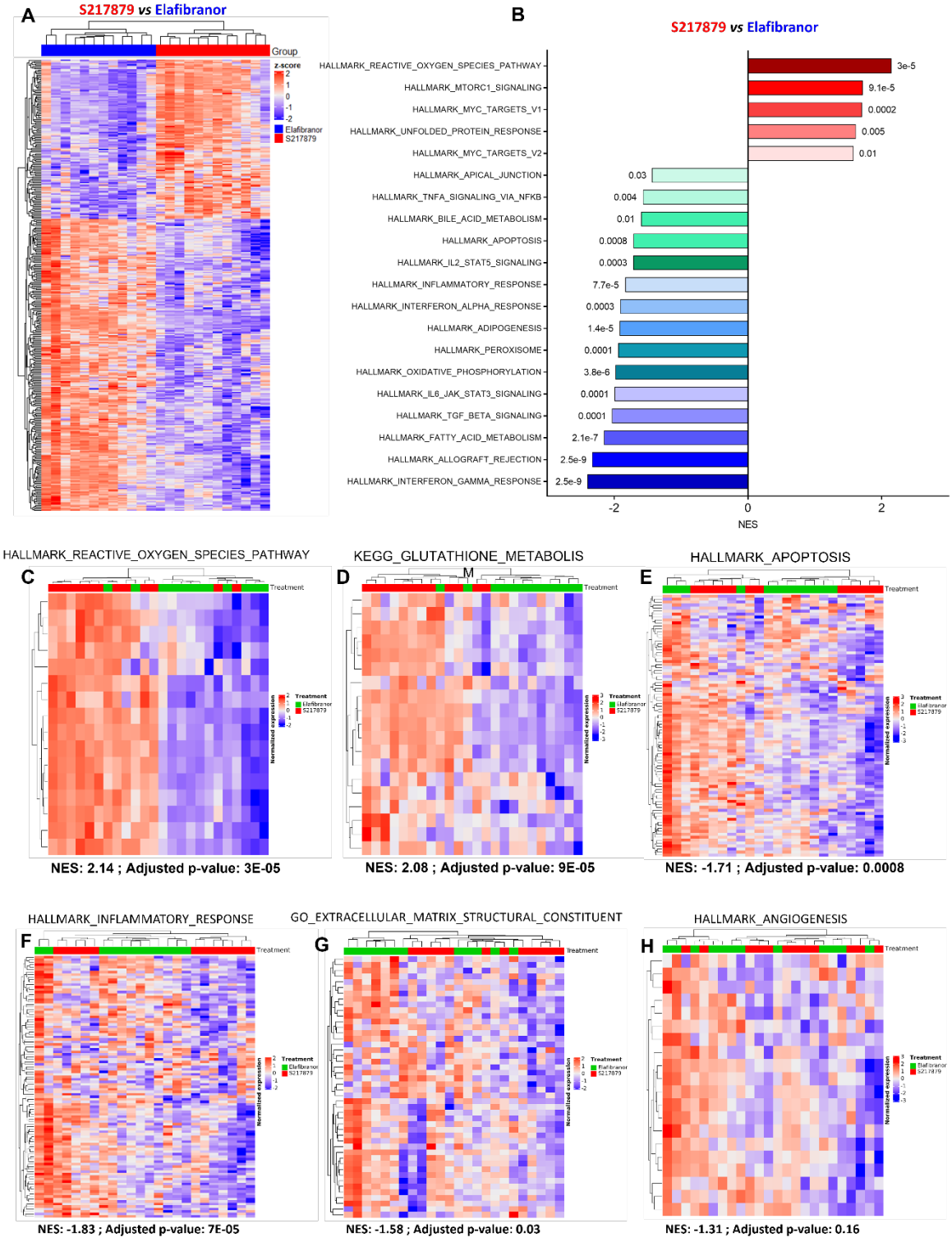

Fig. S9: S217879 has more pronounced effects than Elafibranor to inhibit pathways involved in NASH. Human PCLS were generated from the liver of patients with MAFLD and treated with Elafibranor (10 µM) or S217879 (3 µM) or vehicle (DMSO, 0.1%) for two days. (**A**) Heatmap of significantly differentially expressed genes from S217879 *vs.* Elafibranor-treated

PCLS (FDR-adjusted p-value cut-off: 0.05). (**B**) Gene set-enrichment analysis of most differentially modulated pathways in S217879 *vs.* Elafibranor-treated PCLS with MAFLD. (**C**) Heatmaps of differentially expressed genes in reactive oxygen species, (**D**) glutathione metabolism, (**E**) apoptosis, (**F**) inflammatory response, (**G**) extracellular matrix structural constituent, and (**H**) angiogenesis pathways in S217879 *vs.* Elafibranor-treated PCLS with MAFLD. n=12 PCLS per condition generated from 12 patients with MAFLD. MAFLD, metabolic associated fatty liver disease; NES, normalized enrichment score; PCLS, precision cut liver slices.

Supplementary tables

Supplementary Table S1. Patients' characteristics

					Non tumoral liver used for PCLS	
Patient n°	**Gender**	**Age**	**Indication for surgery**	**Alcohol consumption**	**SAF** [2]	**NAS** [6]
1	F	67	Liver metastases from colon adenocarcinoma	No	S2A1F1	2+0+1=3
2	F	65	Cholangiocarcinoma	No	S1A3F4	1+1+2=4
3	M	65	Hepatocellular carcinoma	Yes	S1A1F3	1+0+1=2
4	F	66	Hepatocellular carcinoma	No	S0A4F4	0+3+2=5
5	M	51	Hepatocellular carcinoma	Yes	S2A3F3	2+1+1=4
6	M	52	Focal nodular hyperplasia	Yes	S1A1F3	1+1+0=2
7	F	67	Non-transplantable liver	No	S1A0F1	1+0+0=1
8	F	48	Neuroendocrine tumor	No	S1A0F1	1+0+0=1
9	M	58	Hepatocellular carcinoma	Yes	S2A3F3	2+1+1=4
10	M	74	Hepatocellular carcinoma	No	S0A3F4	0+1+1=2
11	F	74	Hepatocellular carcinoma	No	S1A4F3	1+2+2=5
12	F	68	Hepatocellular carcinoma	Yes	S1A3F4	1+1+2=4

Abbreviations: NAS, NAFLD activity score; SAF, steatosis, activity, fibrosis score; PCLS, precision cut liver slices.

Supplementary Table S2. Patients' metabolic and morphological features

Metabolic and morphological features	
Age (years)	65.5 (53.5 - 67.7)
Female gender (n, %)	7 (58.3 %)
BMI (Kg/m²)	30.4 (29.3 - 34.7)
Type 2 diabetes (n, %)	6 (50 %)
Fasting serum glucose (g/L)	1.53 (1.20 - 2.40)
Serum AST (IU/L)	46.0 (32.0 - 57.0)
Serum ALT (IU/L)	47.0 (24.0 - 68.0)
Serum gamma-GT (IU/L)	108.0 (37.0 - 125.0)

Abbreviations: ALT, alanine aminotransferase; AST, aspartate aminotransferase; BMI, body mass index; gamma-GT, gamma-glutamyl transpeptidase. n=12 patients. Data are expressed as median ± IQR or n (%) for the gender and type 2 diabetes.

Supplementary Table S3. Characteristics of patients used for autophagic flux evaluation after Elafibranor or S217879 treatment with choloroquine

				Non tumoral liver used for PCLS	
Patient n°	**Gender**	**Age**	**Indication for surgery**	**SAF**	**NAS**
1	F	67	Rejected liver graft	S1A0F1	1+0+0=1
2	F	42	Liver metastases from colon cancer	S1A0F0	1+0+0=1
3	M	65	Vesicular adenocarcinoma	S0A0F0	0+0+0=0
4	F	48	Neuroendocrine tumor	S1A0F1	1+0+0=1
5	M	84	Hepatocellular carcinoma	S0A0F0	0+0+0=0
6	M	58	Hepatocellular carcinoma	S2A3F3	2+1+1=4
7	M	74	Hepatocellular carcinoma	S0A3F4	0+1+1=2
8	F	74	Hepatocellular carcinoma	S1A4F3	1+2+2=5
9	M	68	Hepatocellular carcinoma	S0A0F4	0+0+0=0
10	F	68	NASH related cirrhosis	S1A3F4	1+1+2=4
11	M	69	Hepatocellular carcinoma	S1A1F3	1+0+1=2

Abbreviations: NAS, NAFLD activity score; SAF, steatosis, activity, fibrosis score. PCLS, precision cut liver slices.

Supplementary Table S4. Taqman probes used for qPCR analyses

Gene	Life technologies Taqman probe ID
18S	Hs03003631_g1
ACOX1	Hs01074241_m1
ACTA2	Hs00426835_g1
CCL2	Hs00234140_m1
CCL5	Hs00982282_m1
COL1A1	Hs00164004_m1
COL1A2	Hs01028956_m1
CPT1A	Hs00912671_m1
FASN	Hs01005622_m1
FGF21	Hs00173927_m1
G6PC	Hs02802676_m1
GAPDH	Hs02786624_g1
GPX2	Hs01591589_m1
GPX3	Hs01078668_m1
GSTA2	Hs00747232_mH
HMOX1	Hs01110250_m1
HPRT1	Hs02800695_m1
IL-1β	Hs01555410_m1
IL-6	Hs00174131_m1
MAP1LC3B	Hs00797944_s1
NQO1	Hs02512143_s1
PDK4	Hs01037712_m1
PPARA	Hs00947536_m1
PPIA	Hs04194521_s1
RAD51	Hs00947967_m1
SREBF1	Hs01088679_g1
XRCC1	Hs00959834_m1

Supplementary Table S5. List of antibodies used for western blots and immunostaining analyses

Antibody anti-	Raised in	Reference	Dilution	WB buffer	IHC buffer
α-SMA	Mouse	Sigma Aldrich A2547	1/1000	TBST milk	-
α-SMA	Mouse	Dako M0851	1/600	-	PBS BSA
Cleaved Caspase-3	Rabbit	CST 9661	1/400	-	PBS BSA
CD68	Mouse	Dako M0814	1/500	-	PBS BSA
CHOP	Mouse	CST 2895	1/1000	TBST milk	-
MGST1	Rabbit	Abcam ab131059	1/1000	TBST milk	-
GPX2	Rabbit	Abcam ab137431	1/1000	TBST milk	-
GSTM2	Rabbit	ABclonal A13496	1/1000	TBST milk	-
GSTT1	Rabbit	Abcam ab199337	1/1000	TBST milk	-
ICAM-1	Rabbit	CST 67836	1/1000	TBST milk	-
LC3-B	Rabbit	CST 2775	1/1000	TBST milk	-
p-H2A.X	Rabbit	CST 9718	1/20000	TBST milk	-
p-H2A.X	Rabbit	Abcam ab81299	1/200	-	PBS BSA
SOD	Rabbit	Abcam ab179843	1/1000	TBST milk	-
STING	Rabbit	CST 13647	1/1000	TBST milk	-
VCAM-1	Rabbit	CST 13662	1/1000	TBST milk	-

Abbreviations: BSA, bovine serum albumin; CST, cell signaling technology; IHC, immunohistochemistry; LC3, light chain 3; PBS, phosphate buffer saline; TBST, tris buffer saline 0.05 tween; WB, western blot.

References

[1] de Graaf IAM, Olinga P, de Jager MH, Merema MT, de Kanter R, van de Kerkhof EG, et al. Preparation and incubation of precision-cut liver and intestinal slices for application in drug metabolism and toxicity studies. Nat Protoc 2010;5:1540–51. https://doi.org/10.1038/nprot.2010.111.

[2] Bedossa P, Poitou C, Veyrie N, Bouillot J-L, Basdevant A, Paradis V, et al. Histopathological algorithm and scoring system for evaluation of liver lesions in morbidly obese patients. Hepatol Baltim Md 2012;56:1751–9. https://doi.org/10.1002/hep.25889.

[3] Dobin A, Davis CA, Schlesinger F, Drenkow J, Zaleski C, Jha S, et al. STAR: ultrafast universal RNA-seq aligner. Bioinforma Oxf Engl 2013;29:15–21. https://doi.org/10.1093/bioinformatics/bts635.

[4] Liao Y, Smyth GK, Shi W. featureCounts: an efficient general purpose program for assigning sequence reads to genomic features. Bioinforma Oxf Engl 2014;30:923–30. https://doi.org/10.1093/bioinformatics/btt656.

[5] Bullard JH, Purdom E, Hansen KD, Dudoit S. Evaluation of statistical methods for normalization and differential expression in mRNA-Seq experiments. BMC Bioinformatics 2010;11:94. https://doi.org/10.1186/1471-2105-11-94.

[6] Kleiner DE, Brunt EM, Van Natta M, Behling C, Contos MJ, Cummings OW, et al. Design and validation of a histological scoring system for nonalcoholic fatty liver disease. Hepatol Baltim Md 2005;41:1313–21. https://doi.org/10.1002/hep.20701.